QUANTUM CHAOS AND NUCLEAR SPECTRA

By

Declan Mulhall

AN ABSTRACT OF A DISSERTATION

Submitted to
Michigan State University
in partial fulfillment of the requirements
for the degree of

DOCTOR OF PHILOSOPHY

Department of Physics and Astronomy

2002

Professor Vladimir Zelevinsky

ABSTRACT

QUANTUM CHAOS AND NUCLEAR SPECTRA

By

Declan Mulhall

The regularities in nuclear spectra, especially the spin-zero ground states of even-even nuclei are usually ascribed to the effect of the nuclear pairing interaction. This is seen to be an incomplete picture. Similar regularities are seen in the spectra of random two-body Hamiltonians. The largely ignored role of geometric chaoticity is shown to be the driving force behind this. A system of N spin-j fermions under the influence of a random two-body angular momentum conserving interaction is studied. The spectra exhibited a propensity for the ground states to have spin-zero or maximum spin. The role of pairing was eliminated unambiguously as the cause. A statistical theory based on equilibrium statistical mechanics was developed and an expression for the equilibrium energy derived. The theory was used to successfully describe the salient features of the ensembles studied.

QUANTUM CHAOS AND NUCLEAR SPECTRA

By

Declan Mulhall

A DISSERTATION

Submitted to
Michigan State University
in partial fulfillment of the requirements
for the degree of

DOCTOR OF PHILOSOPHY

Department of Physics and Astronomy

2002

ABSTRACT

QUANTUM CHAOS AND NUCLEAR SPECTRA

By

Declan Mulhall

The regularities in nuclear spectra, especially the spin-zero ground states of even-even nuclei are usually ascribed to the effect of the nuclear pairing interaction. This is seen to be an incomplete picture. Similar regularities are seen in the spectra of random two-body Hamiltonians. The largely ignored role of geometric chaoticity is shown to be the driving force behind this. A system of N spin-j fermions under the influence of a random two-body angular momentum conserving interaction is studied. The spectra exhibited a propensity for the ground states to have spin-zero or maximum spin. The role of pairing was eliminated unambiguously as the cause. A statistical theory based on equilibrium statistical mechanics was developed and an expression for the equilibrium energy derived. The theory was used to successfully describe the salient features of the ensembles studied.

To my family William, Elizabeth, John, Gerard and Desmond Mulhall, and Jennifer

Greene.

ACKNOWLEDGMENTS

Table of Contents

List of Tables

List of Figures

Chapter 1

Introduction

Classical nonlinear dynamics became the poster-child of the physics community with the advent of the computer. Numerical experiments, impossible without a computer, in the 1960's led to some remarkable discoveries. The so called "Butterfly effect" of Lorentz [29] arising from the sensitive dependence on initial conditions of a particular set of nonlinear equations, and the subsequent "strange attractor" in phase space, and Feigenbaum's work on pitchfork bifurcations were among the exciting topics of this period. Laboratory studies of turbulence and convection currents and other nonlinear phenomena were producing interesting results. The Russian physicist Chirikov, in his studies of the beam instabilities in accelerators, established criteria of the exponential divergence of trajectories in Hamiltonian dynamics [10]. This was a boom time for the growing field of classical chaos, and by the mid 1980's the field had captured the imagination of the general public, as is evidenced by the number of popular articles on the topic and the huge success of popular books like Gleick's *Chaos: the making of a new science* [22] which was short-listed for both the Pulitzer prize and the national book award. The world of art (and kitsch) was affected also. Peitgen [37] made an industry based on churning out images of fractals and the (by then ubiquitous) Mandelbrot set [31].

The situation in quantum physics was quite different. The key question is what proper-

ties of a quantum system indicate that the corresponding classical system will be chaotic. The quantities of interest in classical chaos have no clear definition in quantum mechanics and are often meaningless (although the notion of a periodic orbit in phase space and a Lyapunov exponent has some meaning in the mean field picture). Taking the classical limit of a quantum system the operations $\lim \hbar \to 0$, $\lim t \to \infty$ do not commute. Where is one to get chaos from the linear Schrodinger equation? The notion of sensitive dependence to initial conditions is not so obvious here as the uncertainty principle makes the notion of distance between trajectories blurry. The answer lies in statistical spectroscopy. This was first studied in quantum systems by the Russian physicist Gurevich in 1939 when he investigated the regularities of level spacings in nuclear spectra [24]. Although Bohr's compound nucleus description [8] is similar to what we call quantum chaos, one could argue that the first application of the ideas of quantum chaos was in the derivation of Bethe's level density formula [5] where a statistical approach was used for the structure of nuclear spin states. What is clear is that the real pioneer of quantum chaos as it is known today was Wigner. He proposed that as the theoretical nuclear Hamiltonian is too complex to be studied directly, the local fluctuation properties of random matrices with the same global symmetries could be studied. Modern random matrix theory was made a separate branch of science by the works of Dyson.

The basic idea is simple. The exact nuclear Hamiltonian is unknown. Even for non-interacting particles the level density is huge just from combinatorics; with interactions exact calculations even in a reasonably truncated space quickly become impossible. In lieu of the real Hamiltonian and assuming that the physical system is both time-reversal invariant and complicated in any basis except for some exceptional ones which form a manifold of measure zero, one can study an ensemble of random real Hamiltonians, the distribution function of which is invariant under any orthogonal transformation (change of basis). This leads us to the Gaussian Orthogonal Ensemble (GOE). The properties of the

GOE can be derived from $P(H) = P(H')$ where $P(H) = \prod_{i \geq j} P_{i,j}(H_{i,j})$ is the probability of a given Hamiltonian and $H' = O^T H O$ is the Hamiltonian in a different arbitrary basis, with O being the transformation matrix and O^T its transpose. This requirement leads to a Gaussian distribution of independent and uncorrelated matrix elements with the standard deviation of the off-diagonal matrix elements being twice that of the diagonal elements. If H is not time reversal invariant, for example a system of charges in an external magnetic field, we come to the Gaussian Unitary Ensemble (GUE). Finally the Gaussian Symplectic Ensemble (GSE) deals with systems with Kramers degeneracy (systems of an odd number of spin-1/2 particles). The study of these ensembles is the main concern of Random Matrix Theory (RMT) [32]. There are other ensembles of interest which will be mentioned later.

The secular (long range) behavior of the level density is not the domain of RMT. Observable quantities can exhibit variations within a few level spacings. These variations, known as fluctuations, are the bread and butter of RMT. The similarities between the fluctuation properties of experimental data and those of the GOE lead us to accept RMT as a working definition of quantum chaos: a quantum system is deemed chaotic if its spectra exhibit the same local fluctuation properties as those of the appropriate Gaussian ensemble. This definition frees us from the need to work backwards from classical mechanics. The connection to classical mechanics is given by the famous Bohigas conjecture [36]: *"Spectra of time reversal invariant systems whose classical analogs are chaotic show the same fluctuation properties as the GOE"*. For systems without time-reversal invariance GOE can be replaced by GUE.

A different point of view is provided by one-body quantum systems. In this situation one can take some classically chaotic systems like a Newtonian particle in a Sinai billiard and look at an analog, for example a microwave cavity. This electromagnetic analog is described by the Helmholtz equation which has a correspondence with the stationary Schrodinger equation. Here the shape of the cavity (billiard) leads to chaotic trajectories,

3

playing the role of weak residual interactions in many-body quantum chaos. Much work has been done in this area of analog systems [41], all in agreement with RMT.

As stated earlier the field of quantum chaos has its origins in nuclear physics. This is no accident because while the spectra involved are very complex and level densities high, individual states can be studied and statistical methods used, the so-called mesoscopic situation. RMT demands a level spacing distribution well approximated by

$$P(s) = \Gamma\left(\frac{\beta+1}{2}\right)^{-1} (\frac{\pi}{2})^{\beta+1} \sqrt{\pi}\, s^{\beta} \exp(-\frac{\pi}{4}s^2) \qquad (1.1)$$

where $\beta = 1, 2$ and 4 for the orthogonal, unitary and symplectic ensembles [32], respectively. The case where $\beta = 1$ gives the famous Wigner distribution. Early studies of neutron resonances agreed with RMT in this respect [7].

At high level densities even weak interactions can be effectively strong compared to the local level spacing. In shell model calculations, parameterizing the interaction strength by $\lambda \in [0, 1]$ a given class of levels (a set of levels with the same quantum numbers) can be studied as a function of λ. A plot of $E(\lambda)$ for all levels in the class shows a turbulent flow of the energy levels [44] with many avoided crossings. At each avoided crossing or level repulsion, the colliding states become mixed. After a few such collisions the states become highly mixed. We are now in the domain of quantum chaos, and statistical quantities like entropy, temperature, spreading width etc. become meaningful [44]. Some individual states in the chaotic regime can be studied. High resolution neutron and proton scattering give us details of quasistationary states for a brief energy range.

One may question the wisdom of comparing physical Hamiltonians to random matrices. In physical systems a natural ordering of the basis is in energy. The two-body interaction used in shell model calculations leads to sparse matrices as states distant in energy are unconnected by the relatively weak interaction strengths. The Gaussian Ensembles on the other hand are everywhere dense, allow all particles to interact through all possible n-body

4

interactions. Furthermore non-zero matrix elements in the physical system are generated by relatively few numbers (interaction parameters) and geometrical quantities (Clebsch-Gordan coefficients). Research on the Two-Body Random Ensemble (TBRE) [43], where only two-body interactions are allowed and the interaction parameters are random Gaussian distributed quantities, still reproduced the fluctuation properties of the GOE. It is important to note that RMT results for local level statistics are largely independent of the precise distribution of the matrix elements. This is a direct consequence of the law of large numbers, as each eigenvalue is a complicated function of these random matrix elements.

A decade after its inception, the applicability of RMT to nuclear spectra was an open issue. In 1963 Dyson and Mehta lamented: "We would be very happy if we could report that our theoretical model had been strikingly confirmed by the statistical analysis of neutron capture levels. We would be even happier if we could report that our theoretical model had been decisively contradicted . . . Unfortunately our model is as yet neither proved nor disproved" [15]. Almost two decades later Haq *et al.* performed a careful and sophisticated analysis on an ensemble of high quality data from neutron and proton scattering experiments [38]. They calculated a selection of RMT statistics and showed that RMT describes nuclear spectra.

There has been a significant practical output from the theory of quantum chaos. Possibly the most elegant example of this is the statistical enhancement of parity violation in nuclear physics, see the review by Flambaum and Gribakin [19]. The basic idea is a very simple mechanism whereby the chaotic structure of eigenfunctions at high energies can enhance the effect of a weak interaction. An informal account of this mechanism follows. Suppose $\Pi = \sum \Pi_{\nu\nu'} a_\nu^\dagger a_{\nu'}$ is an operator that mixes states of different parity, for example $|s\rangle$ and $|p\rangle$. Near the ground state

$$\langle p|\Pi|s\rangle \sim \frac{\Pi_{sp}}{E_p - E_s} \sim 1 \text{ in some units.} \tag{1.2}$$

At high excitation energies the wave functions are chaotic, and $|s\rangle = \sum_i C_i^s |i\rangle$, with the same for $|p\rangle$. The assumption of chaos means $|C_i^s| \sim |C_i^p| \sim 1/\sqrt{N}$ where N is the number of significant components in the wave function. Writing Π in the second quantized form we have

$$\langle p | \Pi | s \rangle \sim \frac{\langle p | \Pi a_\nu^\dagger a_{\nu'} | s \rangle}{E_p - E_s}$$

$$= \frac{\Pi \sum_i C_i^p C_{i'}^s}{E_p - E_s} \, ,$$

where i and i' are simple states connected by the single-particle operator $a_\nu^\dagger a_{\nu'}$. Already, because of the high level density there is a huge enhancement from the small size of $(E_p - E_s)$. But a further enhancement comes purely from the assumption of chaotic wave functions as $\sum_i C_i^p C_i^s$ is the incoherent sum of N terms of order $1/N$ which is $1/\sqrt{N}$. On the other hand, the typical size of the matrix element between two regular (non-chaotic) wave functions is $1/N$. Thus an enhancement of $\sqrt{N}$, typically $10^2 - 10^3$ is achieved.

Another practical application by Kilgus *et al.* [42] is in spectroscopy. In an experiment with insufficient resolution, the assumption of a Wigner level spacing distribution and Porter-Thomas distribution of multipole strengths makes possible a statistical analysis to recover the missing strengths.

The complexity of a wave function

$$|\alpha\rangle = \sum_k C_k^\alpha |k\rangle \tag{1.3}$$

in some physically preferred (unperturbed or shell model) basis, $\{|k\rangle\}$, can be measured by the basis-dependent Shannon (or information) entropy

$$I_\alpha = -\sum_k w_k^\alpha \ln w_k^\alpha \tag{1.4}$$

where $w_k^\alpha = |C_k^\alpha|^2$. Shannon entropy, being sensitive to N_α, the number of significant components of $|\alpha\rangle$, is a measure of the delocalization of the wave function in $\{|k\rangle\}$. Izrailev

[26] defines the localization length of $|\alpha\rangle$ as the ensemble average of $l_\alpha = \exp I_\alpha$. In the GOE limit, because of orthogonality constraints, $l_\alpha = 0.48N$, whereas a fully delocalized wave function would have $l_\alpha = N$. Zelevinsky *et al.* [44] showed that for shell model eigenstates l_α approaches the GOE value, but does not reach it for realistic interactions. Being basis-dependent, the Shannon entropy by itself is not an indication that a wave function is chaotic. Collective excitations have coherent components, and their wave functions are not chaotic. Enders *et al.* [27] used this point in their study of the level spacing distribution $P(s) = \exp(-s)$ of the scissors mode in heavy nuclei. Their observation of a Poissonian distribution for $P(s)$ lead them to conclude that this mode is collective in nature.

A useful quantity for analysis of wave functions in this situation is the strength function $F_k(E)$ [44] of a simple mode $|k\rangle$ or *local density of states*, LDOS, as it is known in condensed matter physics,

$$F_k(E) = \sum_\alpha w_k^\alpha \delta(E - E_\alpha). \tag{1.5}$$

Experimental data do not resolve dense individual states, so $F_k(E)$ is an important tool for connecting experiment to the theory of quantum chaos. Frazier *et al.* [34] established the generic shape of the strength function of shell model states: Gaussian at the center with exponential tails. Suppressing the interaction strength, they observed a return to the Breit-Wigner shape. The transition between these two regimes was explained by them in agreement with the theory of quantum chaos. The exponential tail of the strength function was exploited by Horoi *et al.* [33] to develop a method of calculating low-lying shell model levels. The method consists of the diagonalization of successfully larger truncations of the Hamiltonian, and extrapolating the values of the lower energy levels, thus avoiding the intense task of diagonalizing the full Hamiltonian.

This leads us to another very important application of quantum chaos. Multiple giant dipole resonances are analogs of zero sound in Fermi-liquids. In nuclear matter, the

7

energy of a single quantum is large compared to the temperature. The widths of pure n-quanta states are estimated by the standard model of strength functions **??** as $\Gamma_n/\Gamma_1 = n$. However, deviations from the standard model and Breit-Wigner shape are amplified in the convolution of strength functions for multiple sequential excitations, leading to an almost-Gaussian strength function. Now the widths are added in quadrature, and $\Gamma_n/\Gamma_1 = \sqrt{n}$, in agreement with experiment.

Wang *et al.* [45], in their study of the structure of the eigenstates and LDOS of a schematic three-orbital shell model found excellent agreement with RMT. They went on to derive analytic expressions for the observed exponential tail of both the eigenstates and the strength function. It is pleasant to note that, in this instance, the classical counterpart of this system is chaotic. An important development in the theory of chaotic wave functions was the statistical theory of Flambaum and Izrailev [17]. Their theory, which considered finite systems of interacting fermions, is based on the properties of chaotic eigenfunctions. A partition function based on the average shape of the eigenstates was developed and from it was derived an expression for the average occupation numbers of the single-particle states.

Until recently, RMT dealt with correlations within a sequence of levels with the same set of quantum numbers. The question of correlations between different sequences in the spectra of random matrices has not been fully investigated. It was noticed by Johnson *et al.* [11], [12], that a rotationally invariant random two-body Hamiltonian showed a surprising regularity in its spectra, namely $J = 0$ occurred as the spin of the ground state with a huge probability. Furthermore they noticed that the gap to the next highest level was much larger than expected. The mean yrast line (mean of the lowest spin-J energy) was parabolic, and claims for vibrational/rotational bands were also made. These are prime examples of inter-sequence correlations. Not surprisingly this work generated a flurry of activity, with many daring suggestions as to the origin of this effect. The undisputed presence of a pairing force in the atomic nucleus was the previously accepted reason for the observed spin-zero

ground state of all even-even nuclei. Now it seemed that other, hitherto unknown, effects could disguise themselves as pairing. Horoi *et al.* [30] compared random and realistic interactions in the shell model and found that while the random interaction generated an abundance of $J^\pi T = 0^+ 0$ ground states, they had small overlaps with those of the realistic interaction, and their $B(E2)$ values were unreasonably small. In short, these chaotic wave functions didn't look similar to realistic nuclear wave functions. Clearly there are many open questions regarding these phenomena.

The purpose of this dissertation is to use the ideas of quantum chaos to shed light on nuclear structure. The main issue is that of the origin of the regularities in nuclear spectra and in particular, the zero spin of the ground state of all even-even nuclei. Conventional wisdom is that specific features of the nuclear interaction explain observed properties of the spectra. This picture is incomplete. Even an ensemble of random Hamiltonians with just global symmetries can have spectral regularities. Such a system is studied here, and after analyzing numerical data and distilling all features of interest, a theory is developed based on equilibrium statistical mechanics which succeeds in explaining many of the regularities. Preceding this, however, is an analysis of neutron resonance data. In the guise of RMT, we use quantum chaos to glean information from neutron resonance data. A more traditional statistical analysis of the neutron resonance widths is also carried out.

Chapter 2 deals with the analysis of neutron resonance data. The data is from four odd-A targets and consists of two sequences of levels with angular momentum J_1 and J_2, in proportions α and $(1 - \alpha)$. The goal is modest, simply to get an estimate of α. Naively, from the $2J + 1$ degeneracy of angular momentum states, one would expect

$$\alpha = \frac{2J_1 + 1}{(2J_1 + 1) + (2J_2 + 1)}. \tag{1.6}$$

The level density is compared to the back-shifted Fermi-gas model, and the results suggest that (1.6) is indeed sensible. Next, the level spacing distribution $P(s)$ is calculated and a

value of α extracted. The results were poor. However, paydirt was hit with the more robust spectral rigidity statistic, $\Delta_3(L)$, where the data and theory agreed nicely. An analysis of the resonance widths follows, where values of α are extracted from the second and third moments of the distribution of widths, based on the assumption of a Porter-Thomas distribution for a single sequence of widths.

Chapter 3 starts with a discussion of randomly interacting fermions, describing the current state of research and posing the main question of the dissertation: *How can a rotationally invariant random interaction generate spectral regularities in the ensemble average ?* The stage is set for the answer with two illustrative examples. The system to be studied, N fermions on a single level of angular momentum j is introduced next. The fermions have angular momentum conserving pairwise random interactions. The striking features of the spectra are described. These include: very high fractions, f_0 and $f_{J_{max}}$, of spin zero and maximum ground state spin, $J_0 = 0$ and J_{max} ; a parabolic yrast line with a pronounced staggering for small values of total angular momentum J_{tot} disappearing for higher values; a Wigner $P(s)$; non-Gaussian distribution of off diagonal Hamiltonian matrix elements; a simple particle-hole structure in the low energy states; smoothly oscillating single-particle occupancies; and finally some very strong correlations between the spin-zero ground states of the $j = \frac{11}{2}$, $N = 4$ and 6 systems.

In chapter 4, a first attempt is made to explain these features; pairs of fermions coupled to angular momentum L are treated as spin-L bosons. An enhancement of f_0 is observed, but not of $f_{J_{max}}$. Then theory based on equilibrium statistical mechanics is developed, with an expression for the equilibrium energy of states with a given angular momentum. The empirical observations of chapter 3 are tackled by the theory. The distribution of ground state spins is well explained, as is the distribution of interaction parameters that give $J_0 = J_{max}$. The equilibrium energies of given angular momentum given by the theory are beautifully correlated with the lowest energies for each value of J_{tot}, differing only by a

constant negative shift in the theoretical energies which disappears for high values of J_{tot}. The ground state wave functions are examined and the role of pairing is addressed. The theoretical single-particle occupancies compare nicely with the empirical values, which oscillate around them. The moment of inertia given by the theory is in excellent agreement with the numerical data, as is the standard deviations of the total level densities.

Appendices are included containing derivations of expressions used in the text.

The main results of this thesis were published in the following:

- **D. Mulhall**, A. Volya and V.Zelevinsky, *Geometric Chaoticity Leads to Ordered Spectra for Randomly Interacting Fermions*, Phys. Rev. Lett. **85** (2000) 4016.

- **D. Mulhall**, V. Zelevinsky and A. Volya, *Spin Ordering of Nuclear Spectra from Random Interactions*, Acta Physica Polonica B, **32** (2001) 2491.

- **D. Mulhall**, A. Volya and V. Zelevinsky, *Random Interactions: Shedding Light on Nuclear Structure*, Nuclear Physics A682 (2001) 229c-235c, **64** (2001).

- V. Zelevinsky, **D. Mulhall** and A. Volya, *Do We Understand the Role of Incoherent Interactions in Many-body Physics*, Physics of Atomic Nuclei, **64** (2001) 579.

Chapter 2

Neutron Resonance Data

Amongst the first successes of RMT was in the 1970's with its application to the Nuclear Data Ensemble (NDE) [43], which was a collection of much of the neutron resonance data available at the time. The data was scant, and a test of RMT on a superposition of two sequences, or a decent statistical analysis of one long sequence of levels was impossible. The current availability of higher quality neutron resonance data provides an excellent opportunity to test the predictions of quantum chaos.

The absorption cross-section of thermal neutrons (neutrons with energy range $0 \sim 10$ keV) show narrow peaks with energy separations ~ 1 eV. The absorbtion peaks broaden until eventually they overlap and become indistinguishable. This phenomenon was the impetus for Bohr's compound nucleus model [8], in which a resonance corresponds to a single-particle configuration with all the kinetic energy concentrated in one neutron. This configuration rapidly melts through residual interactions into a chaotic nuclear wave function. Thus, neutron resonances correspond to eigenvalues of the full nuclear Hamiltonian, and neutron resonance data furnish us with a portion of the nuclear spectrum at high level densities, where quantum chaos reigns.

The angular momentum of the resonance will be a sum of that of the incident neutron, j_n, and the target nucleus, j_N. For low energy neutrons, the orbital angular momentum will

be predominantly zero so $j_n = 1/2$ and the total angular momentum j_T can have one of two values, $j_T = j_N \pm 1/2$. A sequence of neutron resonances, from experiments not sensitive to polarization observables, on odd-A targets is a superposition of two pure sequences of eigenvalues. A fraction α will have angular momentum j_1, and a fraction $(1 - \alpha)$ will have angular momentum j_2, (see Eq. (1.6)).

With this in mind, data for ^{239}Pu, ^{241}Pu, ^{233}U and ^{235}U neutron resonance reactions at Los Alamos National Laboratory and RIKEN was analyzed. The data came in the form of a list of triples $\{E, J, \Gamma\}$ containing the energy of a level, E, its spin assignment, J, and its width, Γ. Our ambitions with the data was were modest, simply to extract the relative density α of spin states using the machinery of RMT. This analysis is described in the remainder of this chapter. The level density was checked against some theoretical models. The distribution $P(s)$ of nearest-level spacings, s, was calculated and from it was extracted α. A $\Delta_3(L)$ analysis was next performed (see section 2.4 for a definition of $\Delta_3(L)$). An analysis of the reduced neutron widths $\Gamma^0 = \Gamma/\sqrt{E}$ yields information on the quality of the data and its consistency with the Porter-Thomas distribution.

Spin assignments were randomly made by the experimentalists, with the exception of the 544 ^{235}U levels in the energy interval $0 \rightarrow 300$ eV. Table 2.1 shows the characteristics of the data sets.

2.1   The Level Density

The Bethe level density formula (based on the Fermi-gas model) remains the foundation for interpreting experimental data. Although it has been elaborated to include states of a given spin J, the assumptions remain the same, namely, independent particles (no residual interaction), equidistant spacing of single-particle states near the Fermi level, ε_f, and the

validity of the saddle-point approximation. The end result is **??**:

$$\rho(E,J) = \frac{\pi}{48} \frac{g_0 (2J+1)}{(6g_0)^{\frac{1}{4}}} \left(\frac{g_0 \hbar^2}{I} \right)^{\frac{3}{2}} \left(E - \frac{J(J+1)\hbar^2}{2I} \right)^{-\frac{7}{4}}$$

$$\exp \left(\sqrt{\frac{2\pi^2}{3} g_0 \left(E - \frac{J(J+1)\hbar^2}{2I} \right)} \right). \tag{2.1}$$

Here $g_0 = \frac{3A}{2\varepsilon_f}$ is the single-particle level spacing and $\varepsilon_f \approx 40$ MeV is the Fermi energy; $I = \frac{2}{5}MR^2$ is the rigid body moment of inertia (M is the nuclear mass); and a nuclear radius R of $1.25A^{\frac{1}{3}}$ fm is assumed, where A is the atomic number. This expression for the level density consistently underestimates the level density calculated from the data, typically by a factor of 10.

While the Bethe formula (2.1) captures the main features of the nuclear level density, in particular the $\exp(\sqrt{AE})$ dependence, it does not include odd-even effects of the mass number A in its assumptions. An improved model was developed, based on the functional form of (2.1) but with added free parameters chosen empirically to improve the fit to experimental data. This model is based on the *conventional shifted Fermi-gas model* developed by Newton and Cameron [46], [35], [9]. The key feature is that odd-even effects are addressed by means of a pairing energy shift where the excitation energy is measured from a fictive ground state energy. The level spacing at the Fermi-level is parameterized by an energy-dependent fitting parameter a. A further refinement is the *back shifted Fermi-gas model*, where the fictive ground state energy is treated as an adjustable parameter Δ.

$$\rho(E,J) = \frac{1}{24\sqrt{2}} \frac{2J+1}{\sigma a^{\frac{1}{4}}} \left(\frac{\exp \left(2a(E-\Delta)^{\frac{1}{2}} - J(J+1)/2\sigma^2 \right)}{(E-\Delta+t)^{\frac{5}{4}}} \right) \tag{2.2}$$

Here t is the thermodynamic temperature defined by $(E-\Delta) = at^2 - t$, and I is the effective moment of inertia. I was calculated, and $\sigma^2 = \frac{It}{\hbar^2} \approx 0.0150A^{\frac{5}{3}}t$. The two empirical

14

	^{239}Pu	^{241}Pu	^{233}U	^{235}U
j_1, j_2	0,1	2,3	2,3	3,4
size	825	237	184	544
α_{th}	0.25	0.42	0.42	0.44
$\alpha_{P(s)}$	0.08	0.0	0.06	0.15
2nd moment				
$\alpha_{\overline{\Gamma^0}}$	0.5	0.5	0.05	0.43
$\overline{\Gamma^0_1}$	1.45	1	-10	0.54
$\overline{\Gamma^0_2}$	0.55	1	1.59	1.35
3rd moment				
$\alpha_{\overline{\Gamma^0}}$	0.13	0.05	0.05	0.42
$\overline{\Gamma^0_1}$	-0.7	1.18	12.21	0.65
$\overline{\Gamma^0_2}$	1.25	0.99	0.41	1.25

Table 2.1: Data characteristics and results for α.

parameters, a and Δ were taken from [46], where two values of each are listed corresponding to I equal to the rigid-body moment of inertia and half the rigid-body moment of inertia. Also, in lieu of actual data, the ^{242}Pu values for a and Δ were used for the ^{240}Pu data. This expression does better, agreeing with the data to within a factor of two.

The rotational kinetic energy term in eq.)2.1) is

$$\frac{J(J+1)\hbar^2}{2I} \approx 10^{-1} \text{ MeV} \tag{2.3}$$

This is tiny compared to the typical neutron separation energy involved, so the ratio

$$\frac{\rho(E, J_1)}{\rho(E, J_2)} \approx \frac{2J_1 + 1}{2J_2 + 1} \tag{2.4}$$

in eq.(2.2), at the neutron separation gives no information about the mixing parameter, α, beyond the naive estimate can be extracted.

2.2 The Level Spacing Distribution

We attempted to extract the mixing parameter α from the level spacing distribution $P(s)$. The statistical arguments and the calculation of the level density suggest that α will be close to $\frac{2J_1+1}{(2J_1+1)+(2J_2+1)}$. We expect the level spacing distribution $P(s)$ to follow the predictions of RMT. In our case we have a superposition of two pure sequences of levels. Again, in the parlance of RMT, a pure sequence is a list of levels with the same quantum number, in this case spin J. Here each sequence is assumed to have

$$P(s) = \frac{\pi}{2} s e^{-\frac{\pi}{4}s^2}, \tag{2.5}$$

the famous Wigner distribution. Two such sequences superimposed, with relative abundances α and $\beta = (1-\alpha)$, are expected to have

$$P^{th}(\alpha,\, s) = e(\alpha s)\, e(\beta s) \left(\alpha^2\, \frac{p(\alpha s)}{e(\alpha s)} + \beta^2\, \frac{p(\beta s)}{e(\beta s)} + 2\, \alpha\, \beta\, \frac{f(\alpha s)}{e(\alpha s)}\, \frac{f(\beta s)}{e(\beta s)} \right) \tag{2.6}$$

where $p(s) = \frac{\pi}{2} s e^{-\frac{\pi}{4}s^2}$, $f(s) = e^{-\frac{\pi}{4}s^2}$ and $e(s) = 1 - \mathrm{Erf}\left(\frac{\sqrt{\pi}}{2} s \right)$. The derivation of this formula is very technical and can be found in [32]. In order to separate the local properties of a spectrum from global (or secular) behavior (for example the $\exp(\sqrt{E})$ increase in the level density,) the spectrum must be unfolded. In its simplest form, which is quite adequate in this case, the unfolding process is simply a matter of expressing each nearest neighbor spacing in terms of the local average. Accordingly, the set of level spacings $\{s_i\}$, were extracted from each spectrum, $\{E_i\}$, by the following unfolding procedure,

$$s_i = n \frac{E_{i+1} - E_i}{E_{i+\frac{n}{2}} - E_{i-\frac{n}{2}}} \tag{2.7}$$

Thus $\{s_i\}$ is just the average spacing over an n-level interval. The results were not so sensitive to the value of n. The procedures were run for $n = 5, 10, 20, 50$ with no noticeable difference in $P(s)$, so a value of $n = 10$ was used. Since, from N levels you only get $N - 2n$ spaces, so a smaller value of n gives better statistics (as there are more spaces).

The spacings, $\{s_i\}$, were binned and the counts per bin dN^{data} were compared with theoretical counts per bin. The theoretical count for a bin bound by s and $s+ds$ is

$$dN^{th}(\alpha) = \int_s^{s+ds} P^{th}(\alpha, s)ds \qquad (2.8)$$

The difference between data and theory for a given value of α is characterized by a number, $\Delta(\alpha)$, which was minimized with respect to α.

$$\Delta(\alpha) = \sum_i (dN_i^{data} - dN_i^{th}(\alpha))^2 \qquad (2.9)$$

The subscript i labels the bins. This scheme was verified for mixtures of GOE spectra and worked well (see Fig. 2.2). However the values of α obtained from the data were very low, (see Table 1).
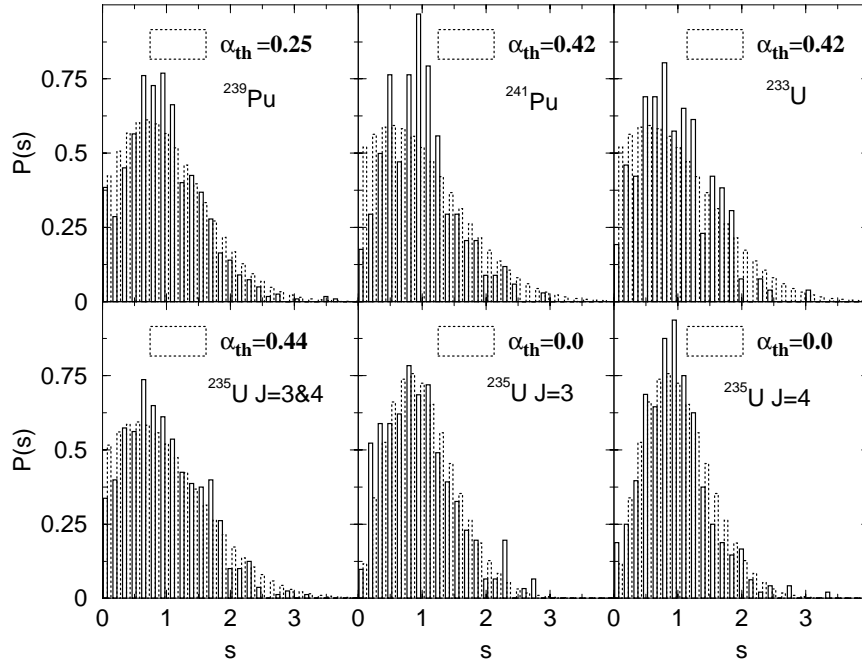
Figure 2.1: The level spacing distribution for each data set. For the ^{235}U data only the first 544 levels were included and an analysis was performed for the $J = 3$ and 4 resonances taken together and separately.

17
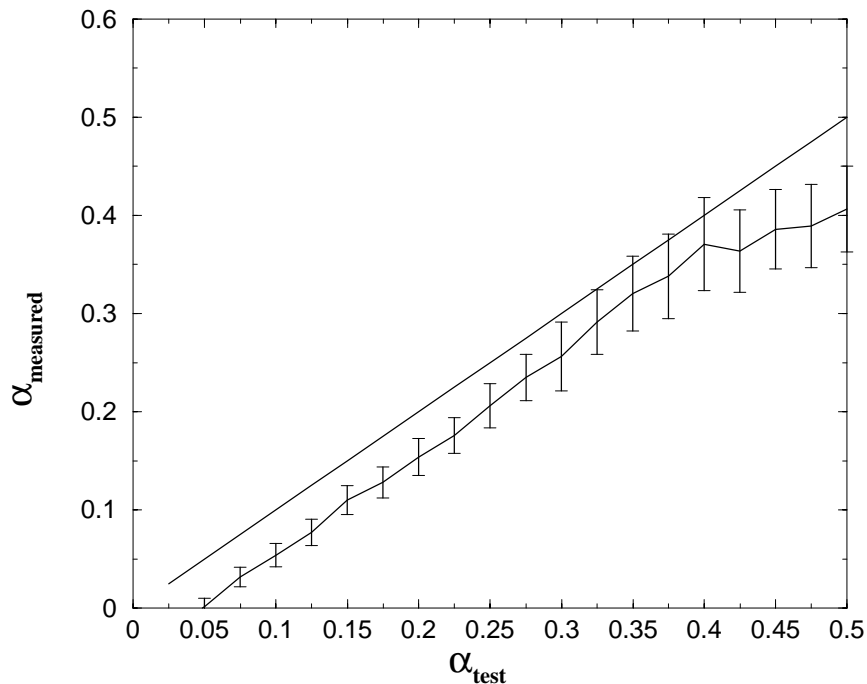
Figure 2.2: The procedure for extracting α from $P(s)$ was tested on GOE spectra ($N = 1000$). The measured values $\alpha_{measured}$ were systematically lower than the actual values α_{test} by approximately 0.05 . However the slope of the graph is unity up to a value of $\alpha = 0.42$

2.3   Spectral Rigidity: the $\Delta_3(L)$ Statistic

The level spacing distribution $P(s)$ of the data gave limited information, but $P(s)$ is sensitive to missed and spurious levels. Another statistic, the spectral rigidity or $\Delta_3(L)$ statistic, is far more robust, being insensitive to missed and spurious levels. The spectral rigidity is a measure of the extent that the unfolded spectrum deviates from a rigid, or picket fence, spectrum. We know that chaotic dynamics lead to level repulsion, hence a rigid spectrum, where the levels "crystalize" . The level of crystallization, or rigidity is measured by $\Delta_3(L)$, which is just the mean deviation of the cumulative level number $N(E) = \int_{-\infty}^{E} \rho(E')dE'$ from a straight line, over an energy interval of length L. The mean is taken with respect to the position of the interval on the unfolded spectrum.

18

$$\Delta_3(L) = \langle min_{A,B} \frac{1}{L} \int_E^{E+L} (N(E') - AE' - B)^2 \, dE' \rangle \qquad (2.10)$$

For regular dynamics where $P(s)$ is Poissonian ($P(s) = \exp(-s)$), $\Delta_3(L) = L/15$. For the GOE, with its Wigner distribution of level spacings, level repulsion means a smaller deviation from a purely rigid spectrum, so $\Delta_3(L)$ is linear for small L and then grows logarithmically for large L,

$$\Delta_3(L) \approx \frac{1}{\pi^2} \left(\ln(2\pi L) + \gamma - \frac{5}{4} - \frac{\pi^2}{8} \right), \qquad (2.11)$$

where γ is Euler's constant. RMT tells us that for a superposition of two pure sequences mixed in proportion α and $\beta = (1 - \alpha)$ we have $\Delta_3(L) = \Delta_3(\alpha L) + \Delta_3(\beta L)$.

Calculations of the $\Delta_3(L)$ statistic are shown in Fig. 2.3. Only for the ^{235}U data is the calculated value value of α consistent with $\frac{2J_1+1}{(2J_1+1)+(2J_2+1)}$. The Pu data sets have a linear $\Delta_3(L)$ which suggest a number of possibilities. Maybe the neutrons weren't just s-wave so more than two spin assignments are required. There may have been missed or spurious levels. There is an additional quantum number in deformed nuclei, namely the K quantum number. If this is conserved there may be more subsequences, for example $K = 0$ for $J_{tot} = 0$ and $J_{tot} = 1$, and $K = 1$ for $J_{tot} = 1$. This would result in 3 subsets, and the fluctuation properties would be closer to those for the Poisson case. The ^{233}U data looks more rigid than one would expect for a mixture of $J = 2$ and $J = 3$ resonances, but it is not clear why.

2.4 The Reduced Width Distribution

The picture of neutron resonances is based on Bohr's idea of a compound nucleus. The neutron is absorbed by the target nucleus. The combination of the target in its ground state and the barely free neutron corresponds to one distribution of energy in the compound
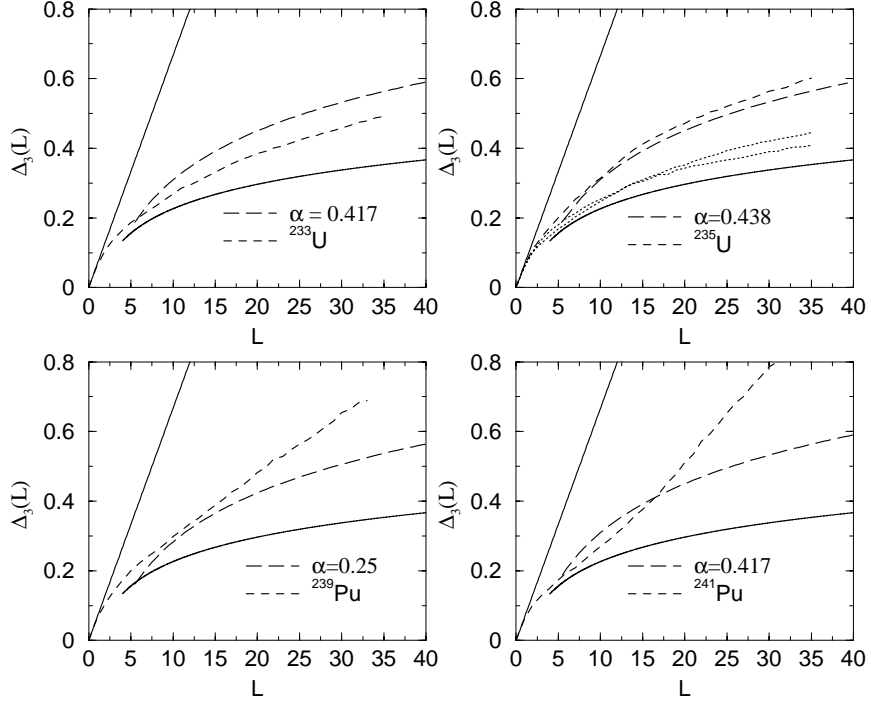
Figure 2.3: The $\Delta_3(L)$ statistic for the data sets. The solid lines in each plot are the RMT results for spectra with the Poissonian level spacing distribution, $\Delta_3(L) = L/15$, and for the GOE (lower logarithmic curve Eq. (2.4)). The long-dashed line in each plot corresponds to the RMT prediction for a superposition of two sequences in the proportions $\frac{2J_1+1}{(2J_1+1)+(2J_2+1)}$.

The short-dashed lines are the results for the data. In the ^{235}U plot the lower dotted lines are the $\Delta_3(L)$ calculations for the $J = 3$ and 4 sequences separately. The ^{235}U data agrees well with the RMT result both for individual sequences and their combination. The ^{233}U data has a logarithmic $\Delta_3(L)$ which looks more rigid than one would expect from simple angular momentum considerations.

nucleus with all the kinetic energy concentrated in one neutron. The kinetic energy of the incident neutron is rapidly spread out. In order to re-emit a neutron, all the kinetic energy must again be concentrated in one particle. This corresponds to a tiny region in phase space. The typical time needed for the excited target to revisit this tiny region is the Poincare recurrence time, whic is quite long, corresponding to a narrow width for this decay mode.

There are two aspects of the physics contained in Γ. On one hand, it is related to the overlap of the target-neutron initial state with the compound nucleus states. The assump-

tion of quantum chaos means that Γ is proportional to the square of Hamiltonian matrix elements, which have a Gaussian distribution. On the other hand, the local density of states for a neutron in the continuum increases as $\sqrt{E}$, as $dp \sim 1/sqrtEdE$. This kinematical effect can be separated from the intrinsic (chaotic) dynamics by studying the *reduced width* $\Gamma^0 = \frac{\Gamma}{\sqrt{E}}$. If

$$P(x) = \frac{1}{\sqrt{2\pi\sigma^2}} \exp(\frac{-x^2}{2\sigma^2}) \tag{2.12}$$

then

$$P(\Gamma^0 \propto x^2) = \frac{1}{\sqrt{2\pi\langle\Gamma^0\rangle\Gamma^0}} \exp(\frac{-\Gamma^0}{2\langle\Gamma^0\rangle}), \tag{2.13}$$

the famous Porter-Thomas distribution which is just a χ^2 distribution with $\nu = 1$ degrees of freedom. Each set $\{\Gamma^0\}$ was scaled so that $\langle\Gamma^0\rangle = 1$ as we are interested in fluctuations. An immediate test on the quality of the data is described in 2.4.1, where $P(\Gamma^0)$ is examined graphically. Then, in section 2.4.2, an attempt is made to extract the mixing parameters α from each data set $\{\Gamma_i^0\}$.

2.4.1 A graphical search for missing levels

The α values extracted from the level spacings are too low compared with the Wigner Surmise. If there were levels randomly deleted or spurious levels detected, or if there were more than 2 sequences of levels in the data, then $P(s)$ would move towards the Poisson limit, and α would look higher then expected, not lower. But if especially close levels were selectively missed, the spectrum could be made to look more rigid than it is.

The data was examined for evidence of missed levels. A convenient method, after Garrison [21], of testing the data for missed levels is to plot $\ln(xP(x))$ vs. $\ln(x)$. These plots are sensitive to the number of narrow widths missed. Narrow levels appear everywhere in the spectrum, as seen in Fig. 2.4, independent of their neighbors. The resulting histograms tell us that if levels were missed, they were missed uniformly in Γ^0. Small Γ^0 were no more

likely to be missed than larger ones.

The assumption that $v = 1$ is not valid for such a superposition. However for the purposes of Fig. 2.4 the difference is not significant. The data was analyzed using the maximum likelihood method. An array of graphs for the datasets is shown in Fig. 2.4.
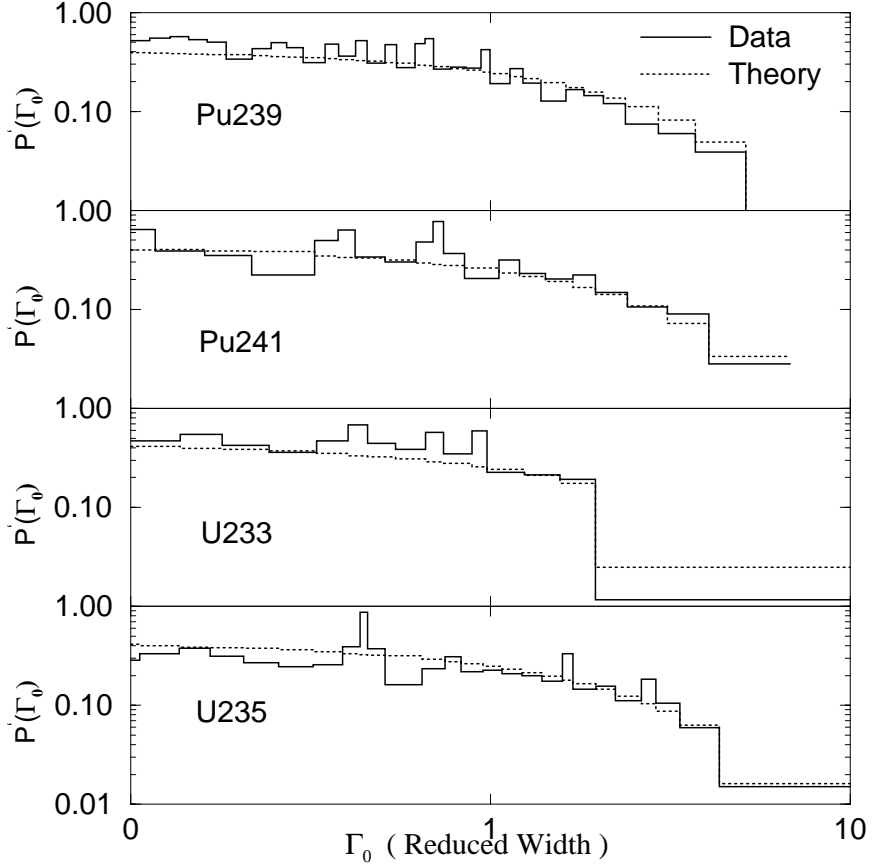
Figure 2.4: The distribution of reduced widths Γ^0 for all four data sets. The dotted line is $P(x) = \chi^2(x|v = 1)$

2.4.2   Higher moments of the reduced widths

The distribution of Γ^0 values is a weighted sum of two Porter-Thomas distributions with means $\overline{\Gamma^0_1}$ and $\overline{\Gamma^0_2}$,

$$P(\Gamma^0) = \alpha P_{PT}(\Gamma^0, \overline{\Gamma^0_1}) + (1 - \alpha) P_{PT}(\Gamma^0, \overline{\Gamma^0_2}). \tag{2.14}$$

22

The nth moment $\overline{x}^n$ of a distribution $P(x)$ of a random variable X is

$$\langle x^n \rangle = \int_{\infty}^{\infty} x^n P(x) dx. \tag{2.15}$$

For the χ^2 distribution with ν degrees of freedom and mean value $\overline{x} = 1$

$$P(x) = \frac{\frac{\nu}{2} x^{\frac{\nu}{2}-1}}{\Gamma(\frac{\nu}{2})} \frac{\nu}{2} e^{-\frac{\nu}{2}x} \tag{2.16}$$

where Γ is the factorial function. The nth moment is

$$\overline{x^n} = \overline{x}^n \left(\frac{2}{\nu}\right)^n \frac{\Gamma(n+\frac{\nu}{2})}{\Gamma(\frac{\nu}{2})} \tag{2.17}$$

The empirical moments of the data can be used to extract the best values of α, $\overline{\Gamma_1^0}$ and $\overline{\Gamma_2^0}$.

$$\overline{\Gamma^{0n}} = 2^n \frac{\Gamma(n+\frac{1}{2})}{\Gamma(\frac{1}{2})} \left(\alpha \overline{\Gamma_1^0}^n + (1-\alpha)\overline{\Gamma_2^0}^n\right) \tag{2.18}$$

After many false leads a procedure was found which gave encouraging (i.e. unambiguous) results. Writing the nth moment of a data set $\overline{\Gamma^{0n}}_{data}$ and the theoretical value calculated with Eq.(2.18) as $\overline{\Gamma^{0n}}_{th}$ (which depends on α and $\overline{\Gamma_1^0}$), a function $\delta(\alpha, \overline{\Gamma_1^0})$ was defined the minimum of which occurred at the optimum values of α and $\overline{\Gamma_1^0}$,

$$\delta(\alpha, \overline{\Gamma_1^0}) = |\overline{\Gamma^{0n}}_{data} - \overline{\Gamma^{0n}}_{th}| \tag{2.19}$$

The initial rescaling of the data to ensure $\overline{\Gamma^0} = 0$ imposed the constraint

$$\alpha \overline{\Gamma_1^0} + (1-\alpha)\overline{\Gamma_2^0} = 1, \tag{2.20}$$

giving $\overline{\Gamma_2^0}$ as a function of $\overline{\Gamma_1^0}$ and α.

$\delta(\alpha, \overline{\Gamma_1^0})$ was evaluated for α in the range $(0.05, 0.95)$ and $\overline{\Gamma_1^0}$ in the range $(.3, 2)$. For each value of $\overline{\Gamma_1^0}$ the value α_{min} of α that minimizes δ was selected and the corresponding triples $\{\delta(\alpha_{min}, \overline{\Gamma_1^0}), \alpha_{min} \overline{\Gamma_1^0}\}$ were saved. A plot of $\overline{\Gamma_1^0}$ *vs.* $\ln\delta(\alpha_{min}, \overline{\Gamma_1^0})$ was made and the value of $\overline{\Gamma_1^0}$ that minimized $\ln\delta(\alpha_{min}, \overline{\Gamma_1^0})$ was read off, see Fig. 2.5. The value of α_{min} was

then read off a graph of α_{min} *vs.* $\overline{\Gamma^0_1}$, see Fig. 2.6. The resulting values of α and $\overline{\Gamma^0_1}$ for the second and third moments of all the data sets are listed in Table 2.1.

The negative values of $\overline{\Gamma^0_{1,2}}$ in Table 2.1 show a breakdown of the method. Once again the procedure worked well for the ^{235}U. For the other data sets no analysis worked. This could be interpreted as an indictment of the quality of the data. These experiments are notoriously difficult to perform.
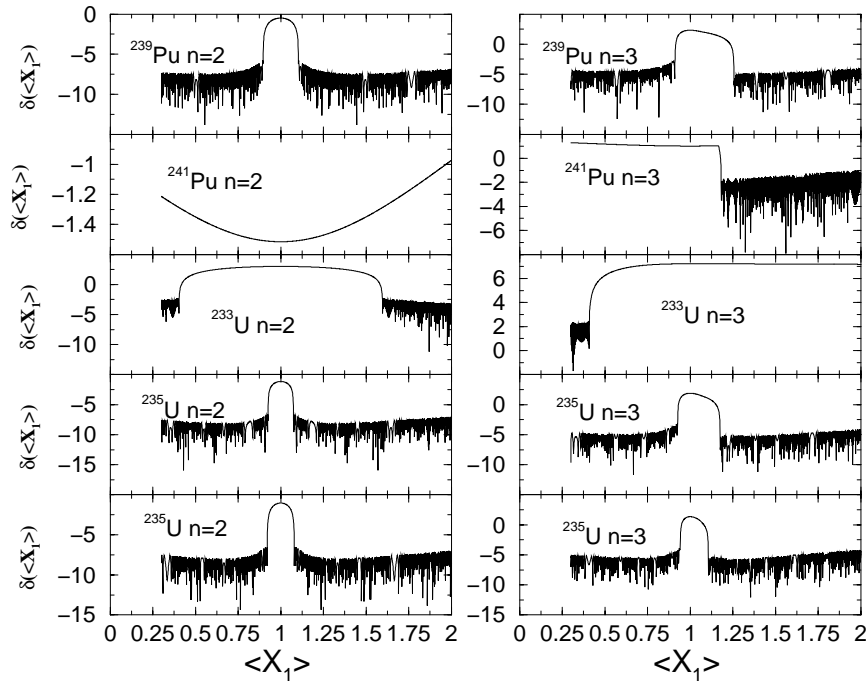
Figure 2.5: The minimum $\ln \delta(\langle X_1 \rangle)$ *vs.* $\langle X_1 \rangle$, (here Γ^0_1 is written as $\langle X_1 \rangle$). The left hand panels correspond to the second ($n = 2$) moment of the data, and the right hand panels correspond to the third ($n = 3$) moment of the data.

24
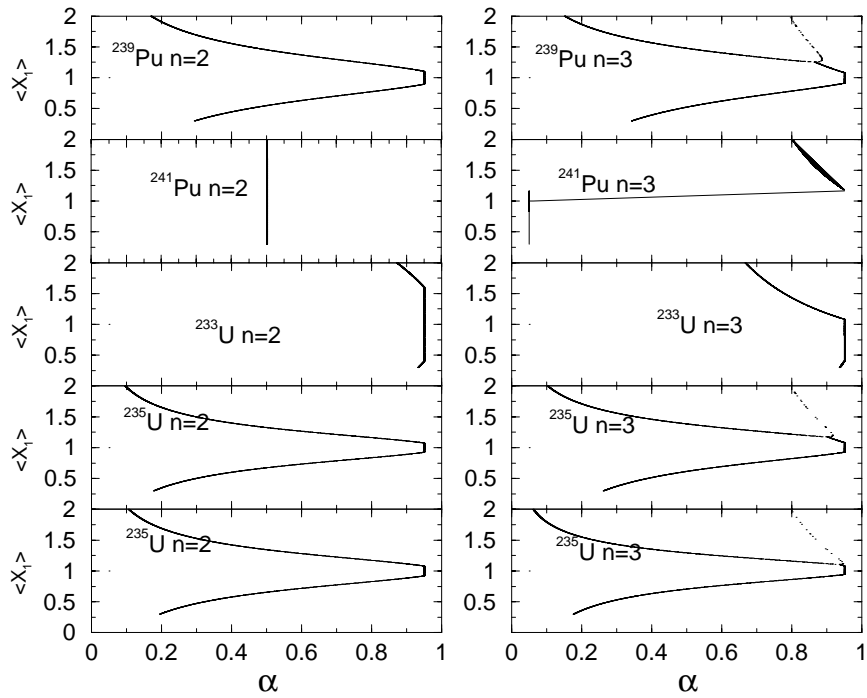
Figure 2.6: The values of α that minimized $\delta(\alpha_{min}, \overline{\Gamma_1^0})$ for a given $\overline{\Gamma_1^0}$ vs. the corresponding

$\overline{\Gamma_1^0}$ (labelled as $\langle X_1 \rangle$ on the y-axis). The values of $\overline{\Gamma_1^0}$ taken from Fig. (2.5) were used here to get the values of α that best fit the data.

Chapter 3

Randomly Interacting Fermions

The complexity of the spectra of many-body systems can originate from completely different sources. There are dynamic and kinematic effects that are fundamentally different. For example, even weak residual interactions at high level densities can give strong mixing of the mean field configurations; this is a dynamic effect. On the other hand, the complexity of states of good angular momentum forces us to treat the coupling of many single-particle angular momenta as a pseudo-random process i.e. not random per se but so hopelessly complicated that it must be treated as such. This kinematic effect leads to geometric chaoticity, introducing immense complexity into our system without any interaction at all. The roles of these disparate effects in shaping spectra are not easily distinguishable.

The standard methods used in understanding global features of nuclear spectra vary with excitation energy. To include angular momentum, the early nuclear level density formulae used this approximation of random coupling of angular momentum, reducing the problem to one of a random walk in the space of the angular momentum projection. Although the concept had not yet been invented, this was the earliest application of quantum chaos. RMT clarified the role of the global symmetries of the Hamiltonian in shaping the local features of the spectra. Its main successes have been in deriving expressions for correlations between levels with fixed quantum numbers for the Gaussian ensembles.

While traditional studies of random spectra concentrate on correlations within such pure sequences of levels, the important question of correlations between different sequences of levels (for example levels with different angular momentum) in random systems has not been thoroughly explored. These correlations could be quite rich in physical information. For example a highly excited deformed nucleus will mix states of the same J. Higher excited states very close in energy but differing in J by one or two unit will probably have a very similar structure, if the energy difference is rotational in nature. This idea led Mottelson to suggest the existence of the so-called rotational compound bands [40] which were seen in the shell model calculations but not yet in nature.

Recently there has been much interest in the spectra of small many-body rotationally invariant systems with a random two-body interaction, stimulated by the work of Johnson et al [11], [12]. They examined such spectra and discovered strong correlations between different J classes. The yrast energies (the lowest energy of spin-J) showed an increase with $J(J+1)$, and a huge probability to have a spin zero ground state. The initial knee-jerk interpretation was that the random interaction effectively had a strong pairing component. They also investigated the distribution of energy gaps in the low-lying levels and claimed evidence of "rotational/vibrational band structures".

There are many interesting results in the flurry of research that ensued. Mulhall *et al.* [14] discovered that in some cases there was also a huge abundance in the number of maximum spin ground states. Furthermore they showed that when the pairing component of the interaction is switched off the excessive appearance of spin zero and maximum spin ground states is only slightly affected. *All* even-even nuclei have $J = 0$ ground states, and this fact is routinely explained by the formation of Cooper pairs. It has been an irresistible temptation to reverse the rule `Cooper pairs give` $J = 0$ `ground states in Fermi systems of even particle number`, and say that $J = 0$ `ground states in Fermi systems of even particle number imply the existence of Cooper pairs`. This is a trap

into which many a researcher has fallen.

The formation of Cooper pairs is intimately related to time-reversal invariance of the Hamiltonian. Bijker *et al.* [6] added a small time-reversal non-invariant component to a random two-body Hamiltonian and observed an increase in the number of $J = 0$ ground states. These observations should put the role of pairing on a less extravagant footing. Zhao *et al.* [47] developed an algorithm for predicting the distribution of ground state spins which sampled the interaction space by taking different L-components individually and merged the results. The intriguing aspect of this is, rather like Samuel Johnson's reaction to a dog walking on its hind legs, not so much that it does it well, but that it does it at all. It is not clear even to the authors themselves why the algorithm works. Horoi *et al.* [30] compared a realistic interaction with a random one in the shell model and found that although the random interaction had a large propensity for $J = 0$ ground states, the states themselves had a small overlap with those of the realistic interaction. Kusnezov *et al.* [13] showed that a system of random interacting bosons in the Interacting Boson Model (IBM) [25] displayed the now familiar excess of $J = 0$ ground states and vibrational/rotational bands, but on comparison with experimental nuclear data there are other physical features not present in the random ensemble, thereby putting constraints on the random systems. Most of the researchers worried about fermionic systems in the dilute limit where the single-particle occupation numbers were small and Pauli blocking was not a strong factor. Santos *et al.* [28] went beyond the dilute limit to show that the regular features of these random spectra were largely independent of whether they were bosons or fermions.

Subsequent investigations found this to be a robust phenomenon with respect to the choice of ensemble (particle number N, single-particle spin j, and distribution of random parameters), being driven by the imposition of a global symmetry. Early on in the drama, a reasonable physical explanation was proposed by Zelevinsky *et al.* [14]. The effect was considered to be a consequence of geometric chaoticity, the complexity of a many-body

state that comes from making a state of good angular momentum. The construction of an N-body wave function of angular momentum J can be performed by coupling a pair of particles to spin-J_{12}, coupling this pair to a third particle to get spin-J_{123} and so on. The choices for the intermediate spins, J_{12} etc., are arbitrary and one scheme is related to another by a unitary transformation whose matrix elements are $3n$-j symbols. Again the reader is reminded that it is this immense complexity of the $|JM\rangle$ states in the M-scheme basis that leaves us with no other choice but to treat the angular momentum coupling as pseudo-random.

To reiterate, the question can be stated as follows: *How can a rotationally-invariant random interaction generate predominantly spin-0 and maximum-spin ground states as well as a smooth yrast line and other non-random features in the ensemble average.* In order to answer this question a randomly interacting system was chosen which is rich enough to exhibit the regular features yet simple enough to tackle analytically. This approach stripped the question of all less important details and allowed us to concentrate on the important aspects of the puzzle.

3.1 A Simple System

Before proceeding any further it is instructive to look at a few simple examples, the first being an analog of the Hund rule in atomic physics. Consider a system of N pairwise interacting spins with the Hamiltonian

$$H = A \sum_{a \neq b} \mathbf{s}_a \cdot \mathbf{s}_b = A[\mathbf{S}^2 - Ns(s+1)]. \tag{3.1}$$

If the interaction strength A is a random variable with zero mean, then the ground state of the system will have equal probabilities, $f_0 = f_{S_{max}} = 1/2$, to have total spin $S = 0$ or $S = S_{max}$ (antiferromagnetism or ferromagnetism).

The second example is the degenerate pairing model [39] where a similar situation takes

place. In this model the pair creation, $P_0^\dagger$, pair annihilation, P_0, and particle number, N, operators form an SU(2) quasispin algebra. Now the eigenenergy is simply proportional to the pairing constant so that, for a random sign of this constant, the ground state quasispin will take a value of 0 corresponding to an unpaired state of maximum seniority, or the maximum possible value corresponding to a fully paired state of zero seniority, with each possibility occurring on average in 50% of cases. For those readers unfamiliar with the argot of pairing, the seniority of a state is simply the number of unpaired particles in that state. In the Elliott SU(3) model [16], as well as in any model with a rotational spectrum, the normal or inverted bands will happen with equal frequency if the moment of inertia takes positive or negative values with equal probability.

Our system is one of N fermions on a single energy level of spin j which has a $2j+1$ degeneracy in the single-particle energies. We are free to choose this system because the regularities we are investigating are robust with respect to the choice of both system and ensemble. Within this space, the general two-fermion rotationally invariant Hamiltonian can be written as

$$H = \sum_{L\Lambda} V_L P_{L\Lambda}^\dagger P_{L\Lambda}, \tag{3.2}$$

where the pair operators for a pair of fermions coupled to spin L and projection Λ are defined as

$$P_{L\Lambda}^\dagger = \frac{1}{\sqrt{2}} \sum_{mn} C_{mn}^{L\Lambda} a_m^\dagger a_n^\dagger, \quad P_{L\Lambda} = \frac{1}{\sqrt{2}} \sum_{mn} C_{mn}^{L\Lambda} a_n a_m; \tag{3.3}$$

a_m annihilates a particle with single-particle angular momentum j and projection m, while $a_m^\dagger$ creates such a particle, $C_{mn}^{L\Lambda}$ are the Clebsch-Gordan coefficients $\langle L\Lambda | jm; jn \rangle$; and the two-particle states $|2; L\Lambda\rangle = P_{L\Lambda}^\dagger |0\rangle$ are properly normalized, $\langle 2; L'\Lambda' | 2; L\Lambda \rangle = \delta_{L'L} \delta_{\Lambda'\Lambda}$. Because of Fermi statistics, only even values of L for the pair operators are allowed in the single-j space, as interchanging the particles gives a phase of $(-1)^{L+1}$. Two particles with projections m_1 and m_2 coupled to angular momentum L interact with energy V_L and leave with projections m_3 and m_4 while the Clebsch-Gordan coefficients ensure conser-

vation of angular momentum at all times. There are $j + \frac{1}{2}$ interaction parameters V_L and these numbers define our ensemble. The ensemble we chose was a uniform distribution of V_L between -1 and 1, which sets the energy scale. The property $P(V_L) = P(-V_L)$ makes attraction and repulsion between particles in a spin-L pair equiprobable. Once again we remind the reader that the results are robust with respect to this choice. In some cases we used Gaussian ensembles, as they are easier to work with analytically.

3.2 Properties of the Operators

Let's look at the properties of the pair operators. This will give useful relations which will be crucial later in the game. In what follows, the fact that L, the angular momentum of the pair, can be only an even integer, will be expressed by means of the factor $\Theta_L = [1 + (-1)^L]/2$ if needed. Also, a factor $\sqrt{2L+1}$ is denoted g_L.

Using the commutation relations and addition formulae for the single-particle creation/annihilation operators a_m and $a_m^\dagger$ in appendix A we get the commutation relations for pair operators of the quasiboson type,

$$[P_{L'\Lambda'}, P_{L\Lambda}^\dagger] = \Theta_L \delta_{L'L} \delta_{\Lambda\Lambda'} + 2\Theta_L \Theta_{L'} \sum_{mm'n} C^{L'\Lambda'}_{jm'\,jn} C^{L\Lambda}_{jn\,jm} a_m^\dagger a_{m'}. \tag{3.4}$$

This can be rewritten in terms of multipole (particle-hole) operators as:

$$[P_{L'\Lambda'}, P_{L\Lambda}^\dagger] = \Theta_L \delta_{L'L} \delta_{\Lambda'\Lambda} \tag{3.5}$$
$$-2\Theta_L \Theta_{L'} g_L g_{L'} \sum_{K\kappa} (-)^K \left\{ \begin{array}{ccc} j & L & j \\ L' & j & K \end{array} \right\} C^{K\kappa}_{L\Lambda L'-\Lambda'} (-)^{\Lambda'} M_{K\kappa}^\dagger.$$

The multipole operators are

$$M_{K\kappa}^\dagger = \sum_{mn} C^{K\kappa}_{jm\,jn} a_m^\dagger a_{-n} (-)^{j-n}, \tag{3.6}$$

and inversely

$$a_m^\dagger a_n = \sum_{K\kappa} C^{K\kappa}_{jm\,j-n}(-)^{j+n} M^\dagger_{K\kappa}. \tag{3.7}$$

Here all values of K from 0 to $2j$ are allowed. The hermitian conjugate gives the standard rule for the multipole moments,

$$M_{K\kappa} = (-)^\kappa M^\dagger_{K-\kappa}. \tag{3.8}$$

The monopole operator, $K = 0$, is proportional to the number of particles N,

$$M_{00} = M^\dagger_{00} = -\frac{1}{g_j}\sum_m a_m^\dagger a_m = -\frac{N}{g_j}. \tag{3.9}$$

The $K = 1$ component is proportional to the angular momentum operator,

$$M^\dagger_{1\kappa} = -\sqrt{\frac{3}{j(j+1)(2j+1)}} J^\dagger_\kappa. \tag{3.10}$$

The relevant commutator is

$$[M^\dagger_{K\kappa}, P^\dagger_{L\Lambda}] = 2g_K g_L \sum_{L'\Lambda'} \left\{ \begin{array}{ccc} j & L & j \\ K & j & L' \end{array} \right\} C^{L'\Lambda'}_{K\kappa L\lambda} P^\dagger_{L'\Lambda'}. \tag{3.11}$$

The operators $\{P_{L\Lambda}, P^\dagger_{L'\Lambda'}, M^\dagger_{K\kappa}\}$ form a closed algebra under commutation, but its too complicated to be practical. For example, for $N = 6$ fermions of spin $j = \frac{11}{2}$ any pair of particles can couple to $L = 0, 2, 4, \ldots 8, 10$ and K can be $0, 1, 2, 3 \ldots, 9, 10$, giving us 253 operators in our algebra.

The Hamiltonian can be identically transformed to the particle-hole (p-h) channel where it is expressed in terms of the multipole operators as

$$H = \varepsilon\hat{N} - \frac{1}{2}\sum_{K\kappa} \tilde{V}_K M^\dagger_{K\kappa} M_{K\kappa}. \tag{3.12}$$

The effective single-particle energy in eq. (3.12) is $\varepsilon = (1/2)\sum_K \tilde{V}_K$, and the interaction matrix elements $\tilde{V}_K$ in the p-h channel ($K = 0, 1, \ldots, 2j = \Omega - 1$ can be both even and odd)

are related to the original matrix elements V_L in the particle-particle (p-p) channel as

$$V_L = \sum_K \left\{ \begin{array}{ccc} j & j & L \\ j & j & K \end{array} \right\} \tilde{V}_K \quad (\text{even } L), \tag{3.13}$$

or, inversely,

$$\tilde{V}_K = (2K+1) \sum_{L\text{even}} (2L+1) \left\{ \begin{array}{ccc} j & j & K \\ j & j & L \end{array} \right\} V_L. \tag{3.14}$$

The transition between the p-p and p-h channels (the so-called Pandey transformation) was studied from the dynamical viewpoint by Belyaev [3]. The channels are complementary in the following sense: the low L components of the p-p channel contribute mainly to the high K components of the p-h channel, and vice versa. The pairing part of the interaction, $L = 0$, corresponds to the sum of all multipole interactions,

$$V_0 = -\frac{1}{\Omega} \sum_K (-)^K \tilde{V}_K. \tag{3.15}$$

This complementarity explains the success of the popular interpolating model "pairing + multipole-multipole interaction" where the effective interaction combines phenomenologically the lowest components in both channels. Note that the interaction parameters cannot be assumed to have the same distributions, $P(V_L) \neq P(\tilde{V}_K)$. $\tilde{V}_K$ are functions of V_L in eq. (3.14), and there are more of them.

The relationship between seniority and the pair-creation/annihilation operators gives us a useful analytical tool. The seniority S of a state is the number of unpaired particles in that state. We are usually interested in $J = 0$ states and will restrict our examples accordingly. Denoting an N-particle seniority-S state by $|S,N\rangle$, possible spin-0 states for an $N = 4$ system are $|0,4\rangle$, $|4,4\rangle$. Notice that $|2,4\rangle$ is impossible because the two remaining unpaired particles must couple to angular momentum zero to have $J = 0$. Similarly for an $N = 6$ particle system the possible $J = 0$ states are $|0,6\rangle$, $|4,6\rangle$, $|6,6\rangle$. $P_0^\dagger$ and P_0 do not change seniority as they create/annihilate a spin-0 pair. A very elegant formalism called "The Quasispin Model" [23] gives us some very useful relations for dealing with senior-

ity eigenstates. In the quasispin model operators are constructed which fulfill the angular momentum commutation rules. Defining

$$S_+ = \sum_{m>0} a_m^\dagger a_{-m}^\dagger$$

$$S_- = \sum_{m>0} a_m a_{-m}$$

$$S_0 = \frac{1}{2} \sum_{m>0} \left(a_m^\dagger a_m + a_{-m}^\dagger a_{-m} - 1 \right).$$

$$(3.16)$$

A simple check shows that these operators commute as the angular momentum operators, J_+, J_-, and J_0. The operator S^2 analogous to J^2 is defined as

$$S^2 = S_+ S_- - S_0 + S_0^2$$

and has eigenvalues $\frac{1}{4}(\Omega - S)(\Omega - S + 1)$ where $\Omega = 2j + 1$. The quasispin model thus gives

$$\langle S, N+2 | P_0^\dagger | S, N \rangle = \sqrt{(\Omega - N - S)(N - S + 2)}$$

$$\langle S, N-2 | P_0 | S, N \rangle = \sqrt{(N - S)(\Omega - N - S + 2)}$$

$$\langle 0, 4 | P_0^\dagger P_0 | 0, 4 \rangle = |\langle 0, 4 | P_0^\dagger | 0, 2 \rangle|^2 = \Omega - 2$$

$$\langle 4, 4 | P_0^\dagger P_0 | 4, 4 \rangle = 0$$

$$|\langle 6, 6 | P_0^\dagger | S, 4 \rangle|^2 = 0 \quad (\text{as } S = 6 \text{ doesn't exist for } N = 4)$$

$$|\langle 4, 6 | P_0^\dagger | 4, 4 \rangle|^2 = \frac{1}{2}(\Omega - 8)$$

$$|\langle 0, 6 | P_0^\dagger | 0, 4 \rangle|^2 = \frac{3}{2}(\Omega - 4).$$

$$(3.17)$$

3.3 The Spectra

A body of empirical information was gathered from numerical simulations in which the eigenvalues and in some cases the eigenvectors of many random Hamiltonians were cal-

culated. A wide range of systems, see Table (3.1), was examined in this way. Direct diagonalization of the Hamiltonian in the m-scheme was used but as the dimensions got large it was necessary to employ the shell model code OXBASH. What follows is a summary of the main features of the ensemble. Some of the figures make reference to "theory". This means the statistical theory developed in the next chapter.

Notations: The ground state spin will be denoted by J_0. The fraction of ground states with spin-J is denoted f_J. D_J is the multiplicity of the spin-value J ($D_{J_{max}} = 1$ for all our systems).

3.3.1 The distribution of ground state spins

The strongest feature of the spectra was the huge incidence of ground states with total angular momentum $J = 0$ (or $J = j$ in the odd-N systems) and $J = J_{max}$, the maximum allowed value, shown in Figs. 3.3-3.5. In the right hand panels of Fig. 3.1 (3.2) the enhancement of $J = 0$ ($J = J_{max}$) states is given as the ratio of f_0 ($f_{J_{max}}$), the observed fraction of spin 0 (J_{max}) ground states, and D_0 ($D_{J_{max}}$), the fraction of allowed values of J that are 0 (J_{max}). This enhancement is clearly large. From the distribution of allowed values of total angular momentum J for a given N and j it is clear that $J = 0$ and $J = J_{max}$ account for a tiny portion of the available states. Moreover, the enhancement of the $J = j$ states for the $N = 5$ system, shown in Fig. 3.4, is consistent with a valence spin j particle on a spin 0 core. It is counterintuitive that a random interaction would generate such a distribution. One would expect something closer to the statistical distribution of allowed values of J.

For the $N = 4$ case there was a staggering of f_0 as j varied which had a period of 3, as shown in Fig. 3.1. Systems with different N were correlated in the sense that the local minima of f_0 (f_j in the $N = 5$ case) occurred at $j = \frac{7}{2}, \frac{13}{2}, \frac{19}{2}$ for all values of N. The origin of this effect lies in the behavior of D_0, the multiplicity of $J = 0$, which for $N = 4$ increases by 1 each time j increases by 3, see Table (3.1).

j	$N=4$	$N=6$	$N=8$	$N=10$	$N=12$
3/2	1	0	0	0	0
5/2	1	1	0	0	0
7/2	2	1	1	0	0
9/2	2	2	1	1	0
11/2	2	3	2	1	1
13/2	3	4	4	2	1
15/2	3	6	7	6	3
17/2	3	8	12	12	8
19/2	4	10	20	24	20
21/2	4	13	31	52	52
23/2	4	16	47	97	127
25/2	5	20	71	177	291
27/2	5	24	102	319	639
29/2	5	29	144	540	1330
31/2	6	34	201	887	2634
33/2	6	40	272	1429	4998
35/2	6	47	365	2219	9113

Table 3.1: The multiplicity D_0, of $J = 0$ for various values of particle number, N, and single-particle spin, j.

3.3.2 The role of pairing

As mentioned in the introduction, the high values of f_0 were initially assumed to be connected in some way to pairing. There is no obvious dynamical reason for the regularities seen in the spectra, yet pairing was assumed by many investigators as a possible culprit. Switching off the pairing interaction by setting $V_0 = 0$ has a very limited effect in the $N = 6$, $j = 11/2$ system. As shown in Fig. 3.6, the value of f_0 did decrease but only by a small amount, from 59% to 55%. Setting $V_0 = -1$ increased f_0 by 25%, but this is hardly unexpected, as the pairing force is now strong and attractive. Of course the $J = J_{max}$ state contains no spin-0 pairs so isn't directly influenced by the value of V_0.

The effect could be kinematical. If the regularities in f_0 are due to random spin coupling, the ground state wave functions are expected to be chaotic and the coherent features of a realistic ground state absent. A point of reference is the totally paired state, $|0, p\rangle$ of
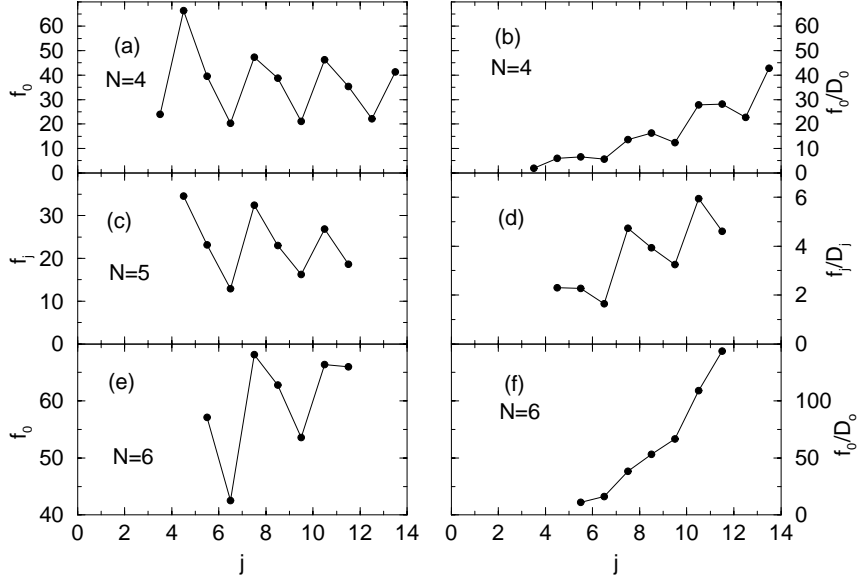
Figure 3.1: The left hand panels (a-c) show values of f_0 (vertical axis) vs the single-particle angular momentum j (horizontal axis). In the right-hand panels f_0 has been divided by D_0, the fraction of the total dimension of the space (ignoring the $2J+1$ degeneracy) accounted for by $J = 0$

seniority zero which would be the ground state for the pure pairing attractive interaction corresponding to a choice of parameters $V_0 = -1, V_{L\neq 0} = 0$. For any set of the parameters from the random interaction ensemble which leads to the zero ground state spin, we calculate the overlap

$$x = |\langle J = 0, \text{g.s.}|0, \text{p}\rangle|^2. \tag{3.18}$$

The histogram of the distribution $P(x)$ is presented in Fig. 3.7(b) for the case of $N = 6$ particles on the $j = 11/2$ level. Clearly, the overlap is very low.

In the extreme chaotic limit the eigenfunctions are expected to be nearly random superpositions of the basis states $|k\rangle$ with the uncorrelated amplitudes C_k constrained only by the orthonormality requirements. The distribution function of the (real) components of a given eigenfunction is the same as that of a multidimensional vector uniformly spread over a unit sphere, $P(\{C_k\}) \propto \delta(\sum_k C_k^2 - 1)$. For the dimension d, this leads to the distribution function of any given component C (a projection of the eigenvector onto a specified direction in
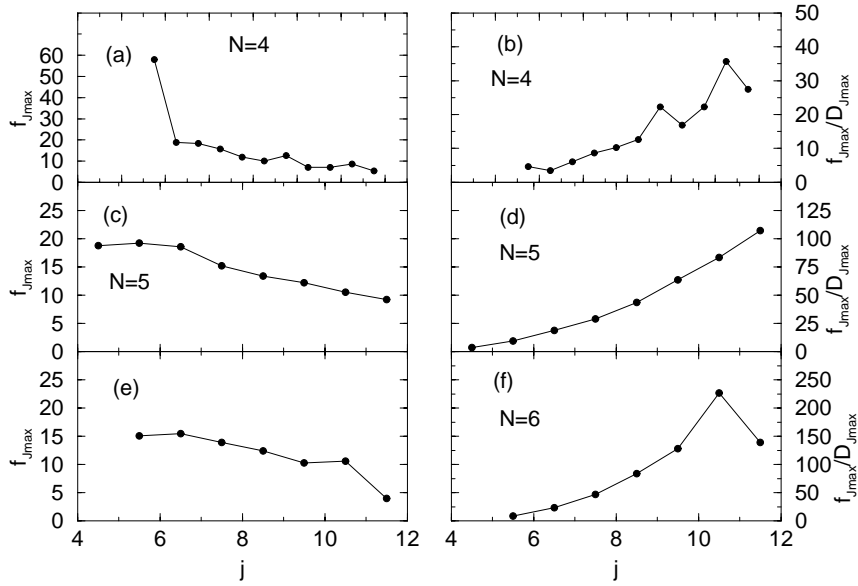
Figure 3.2: Same as Fig. 3.1 but this time we show $f_{J_{max}}$

Hilbert space)

$$P(C) = \frac{\Gamma(d/2)}{\sqrt{\pi}\Gamma[(d-1)/2]}(1-C^2)^{(d-3)/2}\Theta(1-C^2). \tag{3.19}$$

In the limit of $d \gg 1$, eq. (3.19) gives the Gaussian distribution with $\langle C^2 \rangle = 1/d$ while the weights $x = C^2$ are distributed according to the Porter-Thomas law. Complicated nuclear shell model wave functions obtained in realistic calculations with no random parameters are close to the chaotic limit. The typical d-dependence can be unfolded [20] into a regular scheme of approximations, the so-called N-scaling, which allows one to classify various processes going through the compound nucleus stage. The statistical enhancement of weak interaction effects observed via parity non-conservation in neutron resonances, described in chapter 1, and [18], is one of the most convincing illustration of statistical regularities seen on the level of individual wave functions.

In our examples the dimensions d are typically not very large, but the statistical features are brought about by random interactions. We can look at the distribution of overlaps (3.19) as the representative of the distribution of components of eigenvectors along the pairing basis vector $|0,p\rangle$. Six particles on a $j = 11/2$ level give rise to $d = 3$ states of spin $J = 0$.
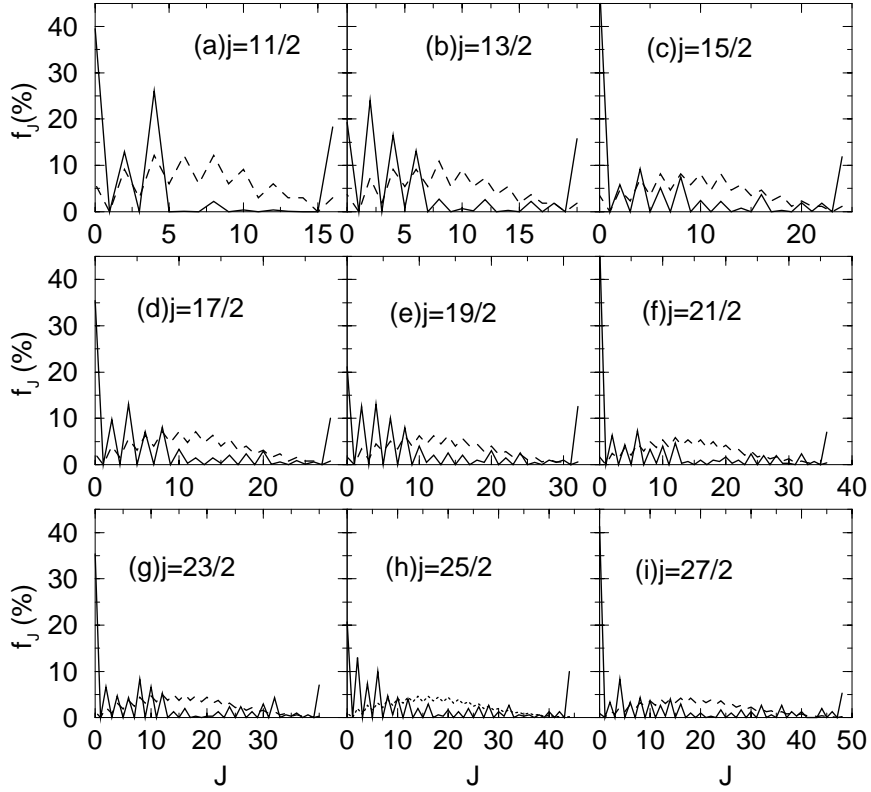
Figure 3.3: The distribution f_J of ground state spins J_0 for various systems of $N = 4$ particles.

In the chaotic limit, this would lead to $P(C) = \text{const}$, and therefore

$$P_{d=3}(x) = \frac{1}{2\sqrt{x}}, \quad 0 < x \le 1. \tag{3.20}$$

This distribution appears in the problem of pion multiplicity from a disordered chiral condensate [1], [2]. This prediction, the dashed histogram in Fig. 3.7(b), is in agreement with the numerical results. Another situation is shown in Fig. 3.7(a) where the data, a solid histogram, are taken for the ensemble which contains regular attractive pairing, $V_0 = -1$, plus uniformly random interactions in all channels with $L > 0$. The presence of pairing generates a significant probability for the paired ground state, a peak at $x = 1$. However, it is possible to show that there exist an "antipaired" state with $J = 0$ but a vanishingly small "probability" to be a ground state so that the space of the candidates for the ground state

39
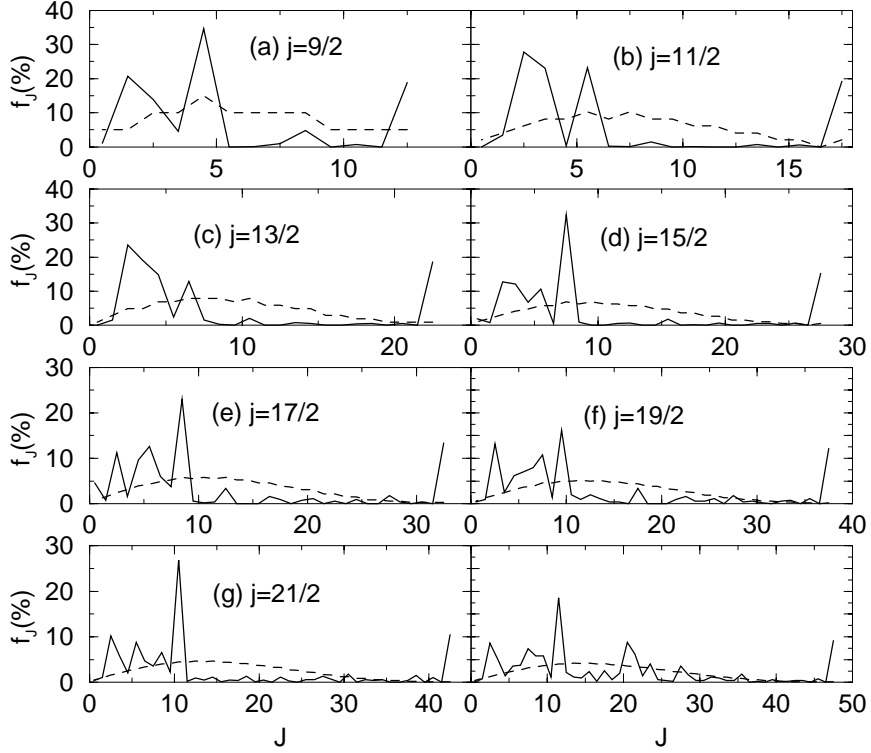
Figure 3.4: The distribution f_J of ground state spins J_0 for various systems of $N = 5$ particles.

position is effectively two-dimensional. For $d = 2$

$$P_{d=2}(x) = \frac{1}{\pi\sqrt{x(1-x)}}, \quad 0 < x \leq 1, \tag{3.21}$$

which agrees qualitatively with the data, Fig. 3.7(a).

3.3.3 The yrast line

Until recently the question of correlations between different classes of levels in random spectra has largely been ignored. RMT has little to say on this topic, yet it is a compelling question. Our ensemble exhibited such a correlation in the form of regular average yrast lines. From the ensemble for each N-body system of spin-J particles, two groups of spectra were extracted, those with $J_0 = 0$ (or j in the $N = 5$ case) and $J_0 = J_{max}$. From these groups the average lowest energy for a given J was extracted. The results for each N, j system were
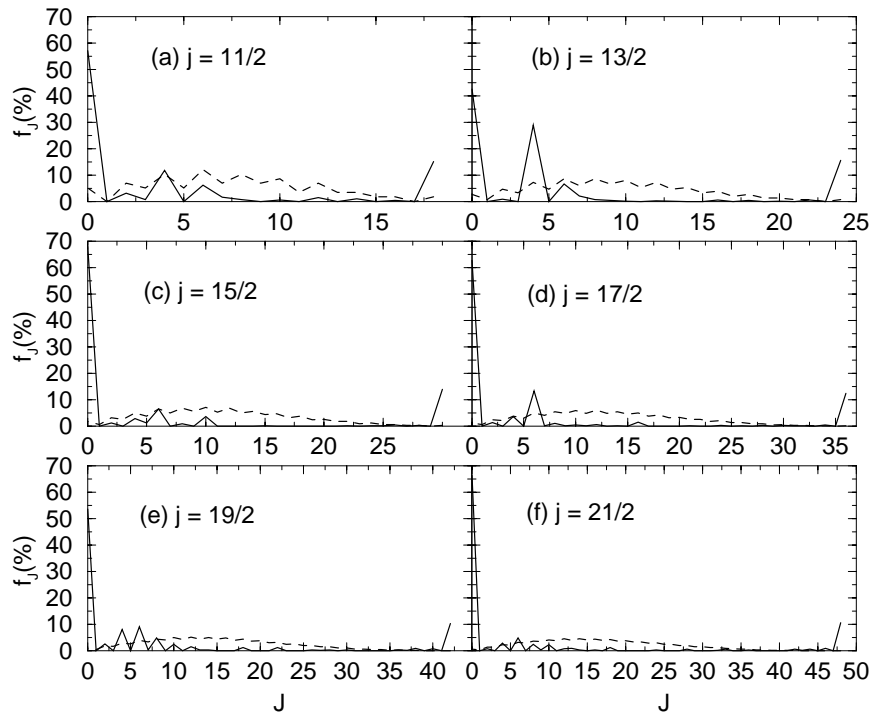
Figure 3.5: The distribution f_J of ground state spins J_0 for various systems of $N = 6$ particles.

fitted to the form

$$E(J) = E_0 + \alpha J(J+1). \tag{3.22}$$

Fig. 3.8 shows the yrast line for a representative system, with the zero of the energy scale taken as the ground state energy. Large fluctuations are especially apparent at small J, with the $J = 0$ and 2 energies, which are on opposite sides of the parabola, while the higher J energies are well approximated by it. This behavior is quite general, being present in all the $N = 4$ and 6 particle systems. Fig. 3.9 refers to the ensemble average of all the six-particle systems.

Any set of V_L will create a mean field which will not, in general, be spherical. This, and the fluctuation of the yrast levels about the parabola, mean that the low lying states are connected by non-collective rotation.

41
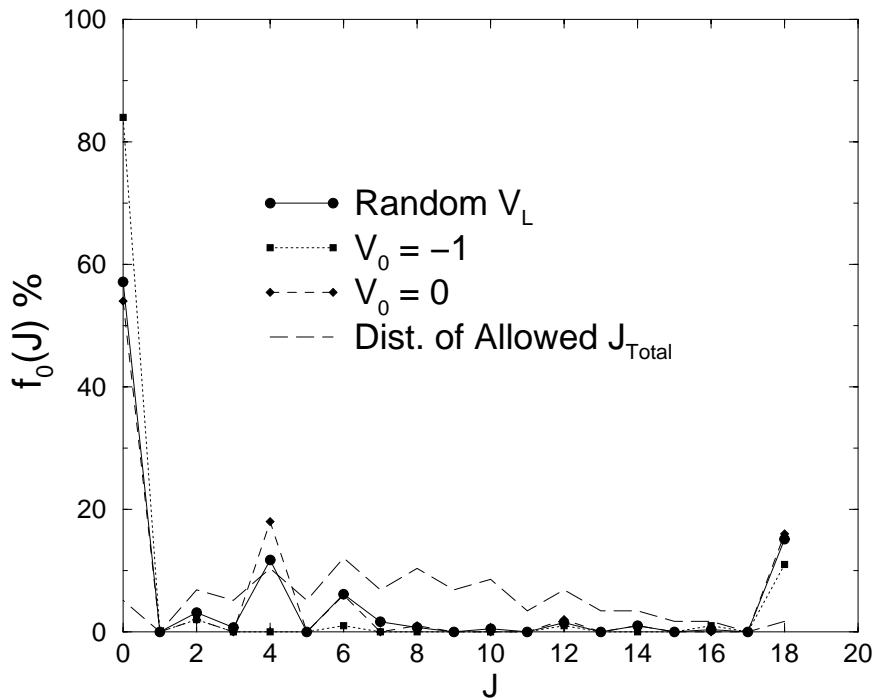
Figure 3.6: f_0 is shown for the $N = 6$, $j = \frac{11}{2}$ system. The cases where the pairing interaction are random or zero are practically indistinguishable.

3.3.4 The ground state energy gap

In even-even nuclei the ground-state is pushed down with respect to neighboring nuclei. This is a result of pairing, but it is not a signature of pairing. Pairing correlations lead to a depressed ground state, but a depressed ground state does not imply pairing.

The energy difference between the ground-state and the first excited state, $E_2 - E_1$, is the ground state gap. The distribution of the ground state gap was compared with the next gap in the spectrum, $E_3 - E_2$. The resulting numbers for each ensemble were divided into three groups corresponding to $J_0 = 0$ (or j for the $N = 5$ cases), $J_0 = J_{max}$, and the rest. The gaps from the first two groups were divided by those of the last group so that they could all be compared sensibly.

The result is that the gaps from the $J_0 = 0$ (or J) sets are larger then those from the $J_0 \neq 0$, J_{max} set, their ratio being consistently close to 2. An examination of the left panels
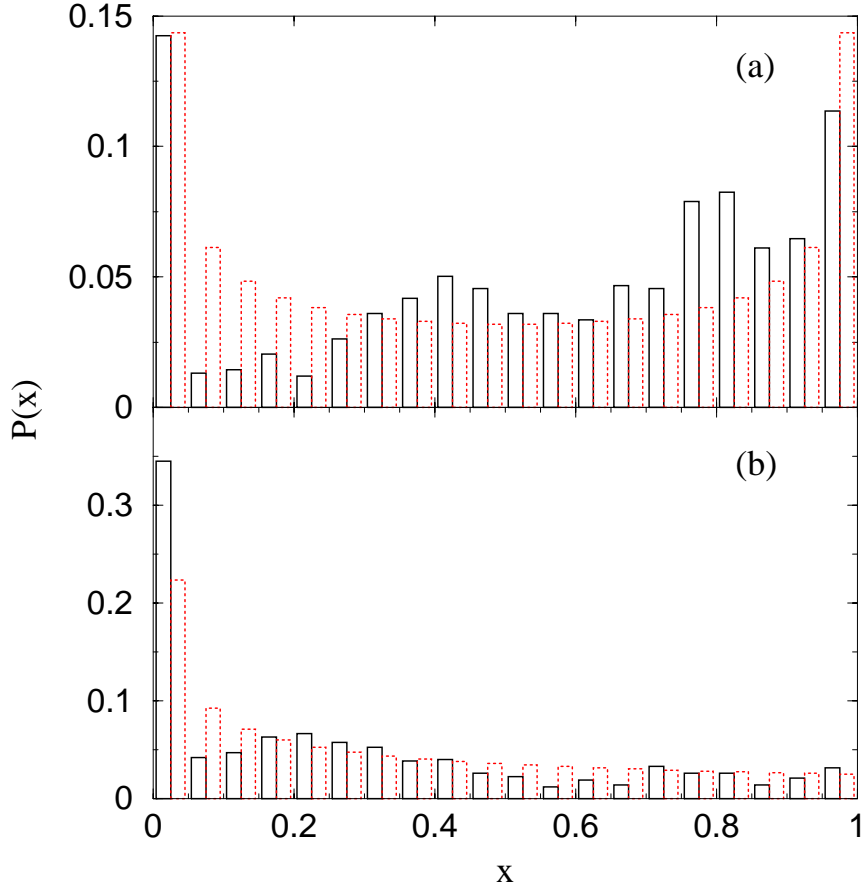
Figure 3.7: The distribution of overlaps, eq. 3.18, of ground states with $J_0 = 0$ with the fully paired (seniority zero) state are shown as solid histograms. Panel (a) corresponds to the ensemble with random $V_{L \neq 0}$ and regular pairing, $V_{L=0} = -1$. Panel (b) corresponds to the ensemble with all V_L random. Dashed histograms show the predictions for chaotic wave functions of dimension $d = 2$, panel (a), and $d = 3$, panel (b).

of Fig. 3.11 suggests that while the pairing force is attractive for these spectra, it is still quite small. Furthermore, the interaction parameters for low L tend to be small or negative. The value of V_0 is not the sole driving force behind the depression of the ground state energy. For a given value of j, there are $j - 1/2$ two-body Slater-determinants with total projection $M = 0$, and there are $j - 5/2$ with total projection $M = \pm 2$. In general there are $(j - 1/2 - L)$ two-body Slater-determinants with total projection $M = \pm L$. This means that a $J_0 = 0$ state is more sensitive to lower-L interaction parameters as more low-L pairs can be involved.
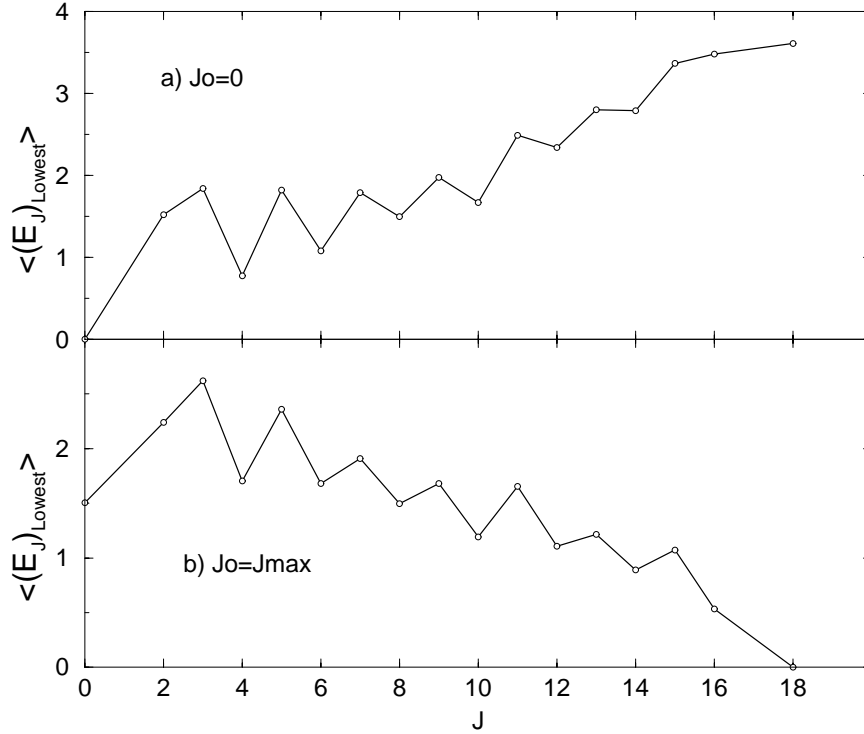
Figure 3.8: The average yrast line for a representative system, $N = 6$, $j = \frac{11}{2}$.

The ratio of gaps from the $J_0 = J_{max}$ sets to those from the $J_0 \neq 0$, J_{max} sets is close to 1; the ground state is not pushed down significantly when $J_0 = J_{max}$. The right panels of Fig. 3.11 indicate that the interaction parameters for high L are large and negative. The ground state energy is not expected to be depressed here because, from simple combinatorics, the J_{max} states cannot form many high-L pairs.

The behavior of the ground state gaps can thus be qualitatively explained an effect of spin projection combinatorics. If this picture is accurate it is another very interesting example of an intra-sequence correlation generated by geometry.

3.3.5 The level density

In our model, we expect the level density for a given class of states with angular momentum J to be Gaussian, centered at 0, and with a standard deviation σ_J, as for the two-body random ensemble (TBRE) [43]. Initially it was suggested that the source of the regularities
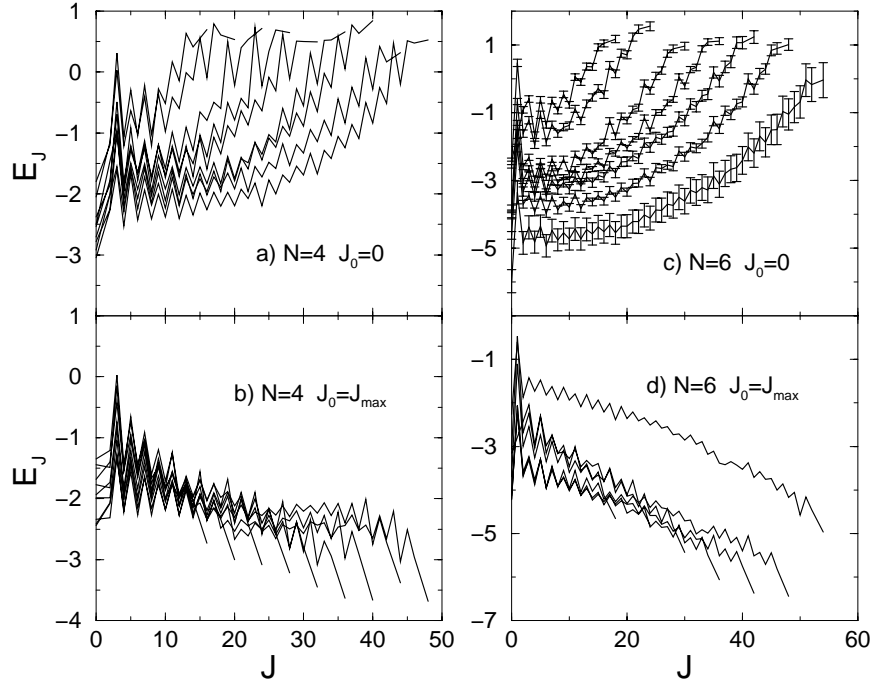
Figure 3.9: The average yrast lines for all the $N = 4$ and 6 particle systems. The range of j starts from 11/2 and goes to 27/2 for $N = 4$, and 21/2 for $N = 6$. The longer lines correspond to systems of higher j. Error bars for 3 panels have been omitted for clarity, but are comparable to those of the $J_0 = 0$ spectra.

in the ground state spin was the behavior of σ_J for the different classes J. If σ_J is dramatically larger for $J = 0$ and $J = J_{max}$, then the ground state would be biased in favor of these values, as the distribution of energies with these spins would stretch to very negative values. Even if this was correct, it would be just a reformulation of the problem rather than an explanation. The actual value of σ_J was extracted from the ensemble by superimposing all the levels of angular momentum J from the spectra, and fitting the resulting normalized distribution, $\rho(E)$, to a Gaussian centered at 0.

Indeed, σ_J is larger for $J = 0$ and $J = J_{max}$ classes, see Fig. 3.12, but the degeneracy, D_J, of these values of J is small, and the effect of the larger size of σ_J is not nearly large enough to explain the distribution of J_0. To illustrate this the following experiment was performed. "Spectra" with the appropriate J degeneracy, D_J, were made, each of the energies generated from a Gaussian distribution centered at 0 and with $\sigma = \sigma_J$, taken from the $N = 6$, $j = 11/2$
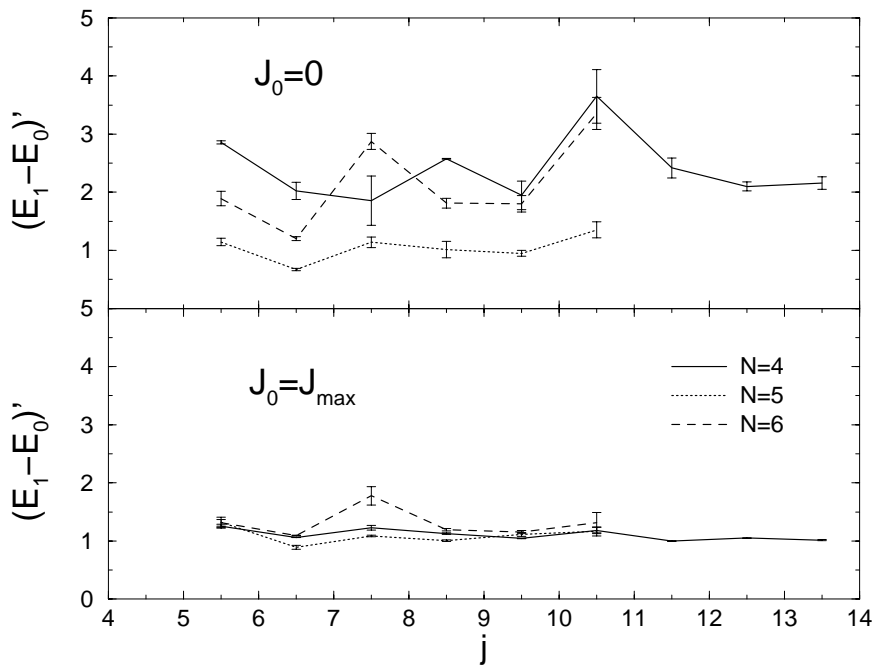
Figure 3.10: The ensemble average ground state energy gaps for all values of *N* and *j*.

ensemble. The resulting f_J is shown in Fig. 3.14. It follows D_J closely until J_{max}. $f_{J_{max}}$ is greater than the statistical weight of J_{max} by a factor of 4. This is the closest similarity to the ensemble result. The conclusion is that σ_J by itself plays no perceivable role in the predominance of spin-0 ground states, but goes some way in explaining the high incidence of J_{max} ground states.

3.3.6 The distribution of level spacings and off-diagonal matrix elements

So far the ground state wave functions have exhibited chaos, and the fluctuations of the yrast states suggested non-collective rotation. Now we come to another signature of chaos, this time on the level of spectral fluctuations within a class of states, namely the level spacing distribution, $P(s)$, discussed in 2.2. To study $P(s)$, a value of J was chosen with large enough D_J to give a dozen or so spacings, the sequence was unfolded and a set of spacings $\{s\}$ extracted. The resulting distribution $P(s)$ agreed well with the parameter-free
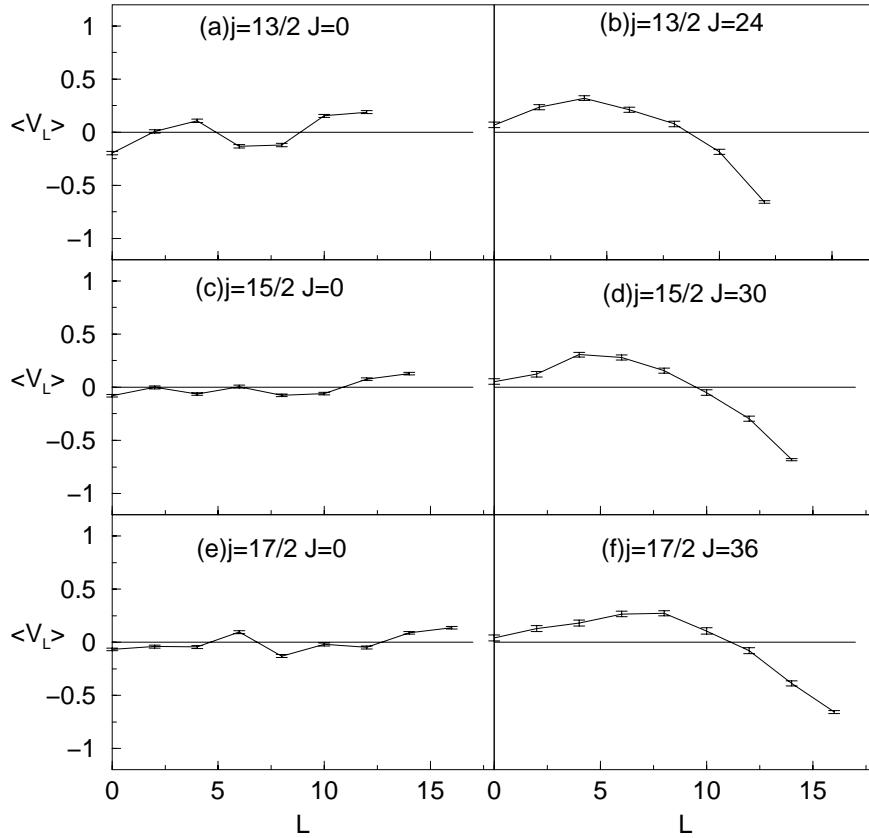
Figure 3.11: The mean value, $\langle V_L \rangle$, of the subsets of $\{V_L\}$ vs. L that give $J_0 = 0$ or $J_0 = J_{max}$, for all the $N = 6$ systems. The panels are labelled with the value of the single-particle spin, j. On the left are the $J_0 = 0$ data, and on the right are the $J_0 = J_{max}$ data.

universal Wigner distribution (1.1), see Fig. 3.15.

The distribution of the off-diagonal matrix elements of the Hamiltonian is Gaussian, as expected from RMT. If the basis is changed from the m-scheme to the $|JM\rangle$ basis, the Hamiltonian is block-diagonal, and orthogonal invariance is lost. The off-diagonal matrix elements in a given block no longer have a Gaussian distribution. In shell model calculations with realistic two-body interactions, the distribution of off-diagonal matrix elements is close to the Porter-Thomas form,

$$P_J(H_{i\neq j}) = \frac{\alpha^{1+q}}{2\,\Gamma(1+q)}\,|H_{i\neq j}|^q\,e^{-\alpha|H_{i\neq j}|}. \tag{3.23}$$

Actually, this distribution arises in a variety of systems, including nuclear and atomic shell models, and may be generic for these many-body interactions [44].

47

Figure 3.12: The standard deviation of the level density, $\rho_J(E)$, of states with total angular momentum J_{Total} for three representative systems.

Our Hamiltonians for the $j = 11/2$, $N = 4$ and 6 systems have $J = 0$ blocks of 2 and 3 dimensions, respectively. The matrix elements in a randomly chosen basis were calculated explicitly in terms of the interaction parameters $\{V_L\}$. To compare $H_{i\neq j}$ from different sets $\{V_L\}$, they must be brought to the same scale. A reasonable scaling procedure is to divide by $\sqrt{\mathrm{Tr}(H - \langle H \rangle)^2}$. Statistically $\mathrm{Tr}(\langle H \rangle) \approx \frac{1}{D_0}\mathrm{Tr}(H)$, where D_0 is the dimension of the $J = 0$ block. Our procedure is to divide each $H_{i\neq j}$ by $\sqrt{\mathrm{Tr}(H^2) + (\frac{1}{D_0^2} - \frac{2}{D_0})\mathrm{Tr}(H)^2}$. As we are concerned with the $J = 0$ block of the Hamiltonian we have an additional quantum number at our disposal, namely S, the seniority. An ordering of the seniority basis is chosen such that the diagonal elements H_{11}, H_{22}, and H_{33} correspond to $S = 0$, 2, and 6 respectively. For $N = 6$ in the seniority basis only H_{12} survives, reason being that according to (3.17), the spin-0 block of H cannot mix $S = 6$ states with $S = 0$ or 4 states and consequently the value of D_0 must be changed to 2. The results for $N = 6$, Fig. 3.16, show that in
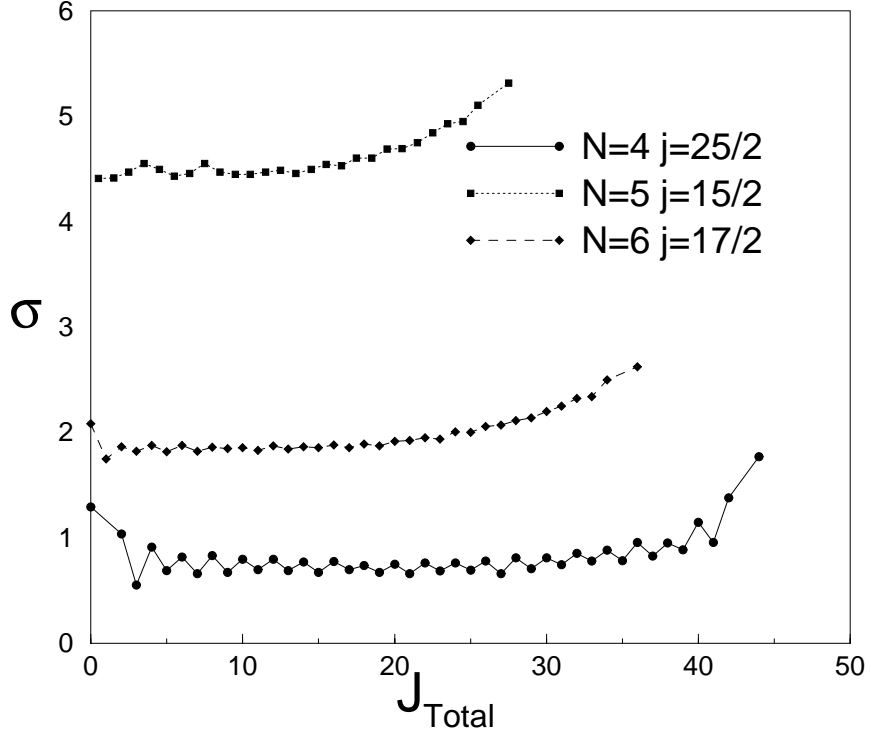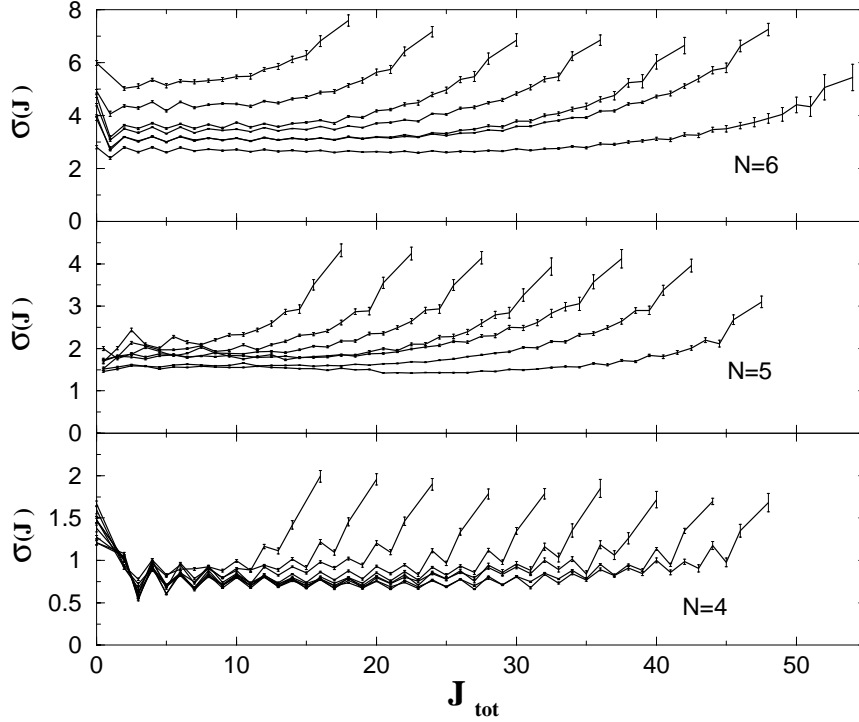
Figure 3.13: The standard deviation of the level density $\rho_J(E)$ of states with total angular momentum J_{Total} for all the systems. The values of j start at 11/2 and increase by one as the lines get progressively longer.

the seniority basis $P(H_{12})$ is far from Gaussian, it is more like a sum of two negative exponential functions, and it is quite close to $P(H_{12})$ for the random basis. In the random basis $P(H_{13})$ and $P(H_{23})$ fall off rapidly, suggesting that the random basis is accidentally close to the seniority basis where H_{13} and H_{23} are zero. In a three-dimensional system such an accident is quite plausible. In the $N = 4$ system the distribution in both bases has two peaks, a surprising result and most likely an artifact of the scaling procedure, see Fig. 3.17. An alternative scaling procedure was tried where H_{12} was divided by $\sqrt{\text{Tr}(H^2)}$. This gave a negative exponential distribution, with $q = 0$ and $\alpha = 1.8$ in (3.23), Fig. 3.18.

3.3.7 Multipole moments and transition collectivity

The structure of the low-lying states generated by random interactions is of interest. We have already seen in section 3.3.2 that the spin-0 ground states are chaotic in nature, hav-
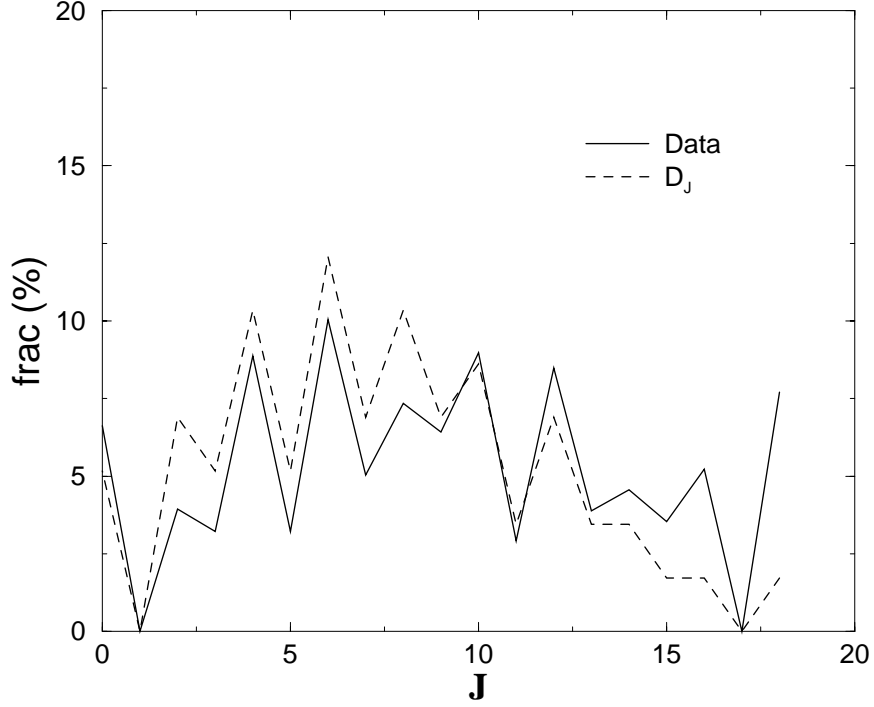
Figure 3.14: The fraction of systems with ground states spin $J_0 = J$ vs J for fake spectra where $\sigma(J)$ is taken from the $N = 6$, $j = 11/2$ ensemble.

ing none of the coherent properties of a physical ground state. Nor do the $J = 0$ ground states have any of the characteristics of a paired condensate. One can ask if the low-lying states are built of single-particle-hole excitations or if, for example, Slater determinants of a particular seniority play a special role in the $J = 0$ ground states. With this in mind the low energy wave functions were probed with multipole operators, $M_{K\kappa}^{\dagger}$, defined by

$$M_{K\kappa}^{\dagger} = \sum_{mn} C_{jm\ jn}^{K\kappa} a_m^{\dagger} a_{-n} (-)^{j-n},\tag{3.24}$$

and the spin-0 pair operators $P_0^{\dagger}$ and P_0. The multipole operators are creation-annihilation operators for particle-hole excitations of a given angular momentum. Here we will define a quantity, $X_K(i \rightarrow f)$, with which we can gauge the collectivity of an excited state in terms of the reduced transition probability. The reduced transition probability between an initial

50
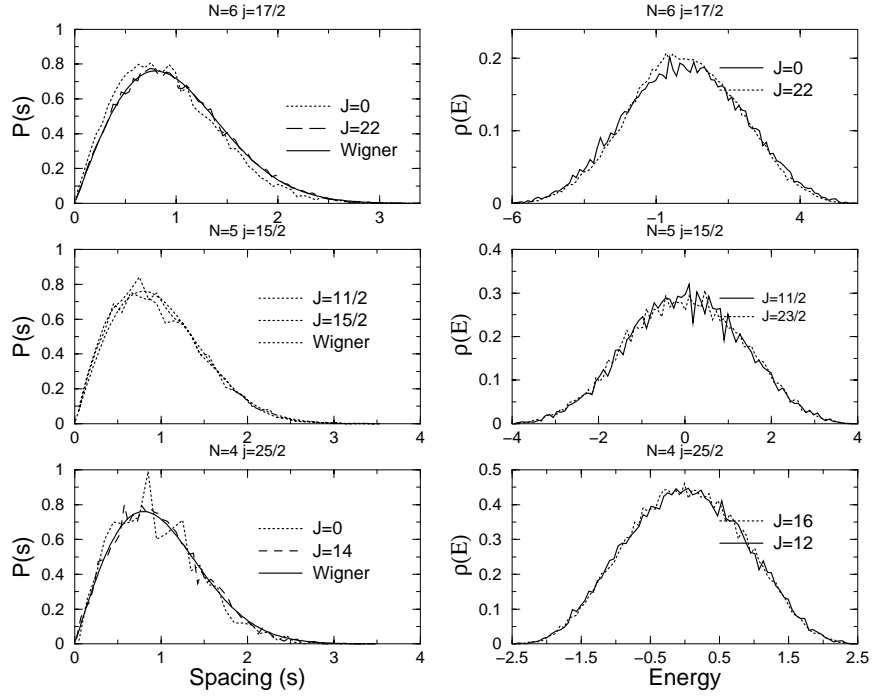
Figure 3.15: The distribution of energies, $\rho_J(E)$, (right panels), and energy spacings, $P_J(s)$, (left panels), with fixed J for three representative systems.

state $|i\rangle$ and a final state $|f\rangle$, $i \to f$, of multipolarity K is defined as

$$B_K(i \to f) = \sum_{M_f \kappa} \left| \langle f J_f M_f | M_{K\kappa}^\dagger | i J_i M_i \rangle \right|^2, \tag{3.25}$$

The average fluctuation of $M_{K\kappa}^\dagger$ in the initial state $|i\rangle$ is

$$S_K[i] = \sum_{f J_f} B_K(i \to f) = \sum_\kappa \langle i J_i M_i | M_{K\kappa} M_{K\kappa}^\dagger | i J_i M_i \rangle. \tag{3.26}$$

The fractional collectivity of a given state, labelled f, is

$$X_K(i \to f) = \frac{B_K(i \to f)}{S_K[i]}. \tag{3.27}$$

$X_K(i \to f)$ will be peaked around 1 if the final state consists of simple particle-hole excitations of the initial state. However, if the lowest $J = 4$ state is connected to a $J = 0$ ground state by $\sum_{\mu\mu'} C_{2\mu 2\mu'}^{4\kappa} M_{2\mu}^\dagger M_{2\mu'}^\dagger$, this would indicate a two particle two hole structure which has more potential for collectivity. The $N = 4, 6$ $j = 11/2$ systems were thus analyzed, and

Figure 3.16: The probability distribution $P(H_{ij})$ of the off-diagonal matrix elements of the 3×3 $J = 0$ block of the $N = 6$, $j = 11/2$ Hamiltonian in the $|JM\rangle$ basis. Except where the seniority basis is specified the basis has been randomly chosen. Note the shoulders on $P(H_{ij})$ in the seniority basis.

there was no evidence of such a structure. The distribution of values of $X_K(i \to f)$ were peaked at unity indicating that the excited states were simple particle-hole excitations.

The J^2 and $\sum_\kappa M_{K\kappa} M_{K\kappa}^\dagger$ matrices were calculated for the $N = 4, 6$ $j = 11/2$ systems. The degeneracy of the $J = 0$ states, D_0, is 2 for the $N = 4$ particle system, and 3 for the $N = 6$ particle system. The $J = 0$ states that maximized and minimized $S_2[0]$ and $S_4[0]$ were made by diagonalizing $\sum_\kappa M_{K\kappa} M_{K\kappa}^\dagger$ in the $J = 0$ block. Having found these states, the single-particle occupation numbers n_m were extracted for each state. The contributions to n_m from Slater determinants of specific seniority were separated. It is immediately clear that the states that maximize $S_2[0]$ and $S_4[0]$ consist mainly of seniority zero Slater determinants, while the states that minimize $S_2[0]$ and $S_4[0]$ mix all seniorities, see Figs. 3.19 and 3.20.

52

Figure 3.17: The probability distribution $P(H_{ij})$ of the off-diagonal matrix elements of the 2×2 $J = 0$ block of the $N = 4$, $j = 11/2$ Hamiltonian in the $|JM\rangle$ basis rescaled according to the prescription in the text.

To further examine the structure of the lowest $J = 4$ states we looked at the operator

$$Q^{\dagger}_{L\Lambda;KK'} = \sum_{\kappa_1,\kappa_2} C^{L\Lambda}_{K\kappa_1;K'\kappa_2} M^{\dagger}_{K\kappa_1} M^{\dagger}_{K'\kappa_2} \tag{3.28}$$

which is just a pair of spin-K particle-hole excitations coupled to angular momentum L.

In analogy with (3.25) and (3.26), we define

$$B_{Q;L}(i \to f) = \sum_{\Lambda} \left| \langle f J_f \Lambda | Q^{\dagger}_{L\Lambda} | 0 \rangle \right|^2 , \tag{3.29}$$

and

$$S_{Q;L}[0] = \sum_{\Lambda} \langle 0 | Q_{L\Lambda} Q^{\dagger}_{L\Lambda} | 0 \rangle. \tag{3.30}$$

Now the same questions we asked about the single-particle-hole excitation nature of wave functions can be asked for two-particle-two-hole excitations. When $B_4(0 \to 4)$ compared to $B_{Q;4}(0 \to 4)$ we see a strong correlation. If one quantity is large, the other is small. This
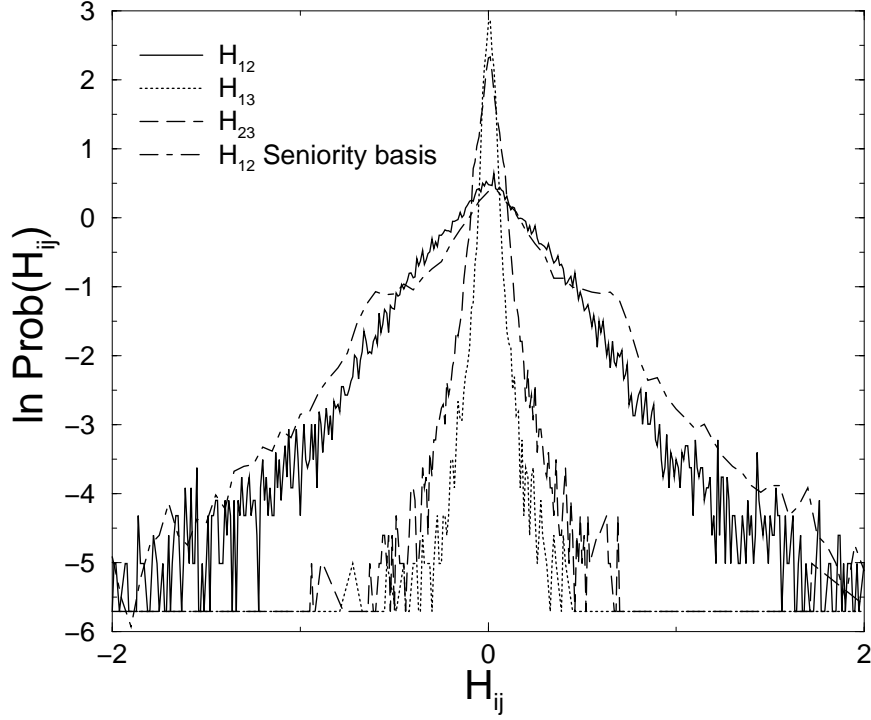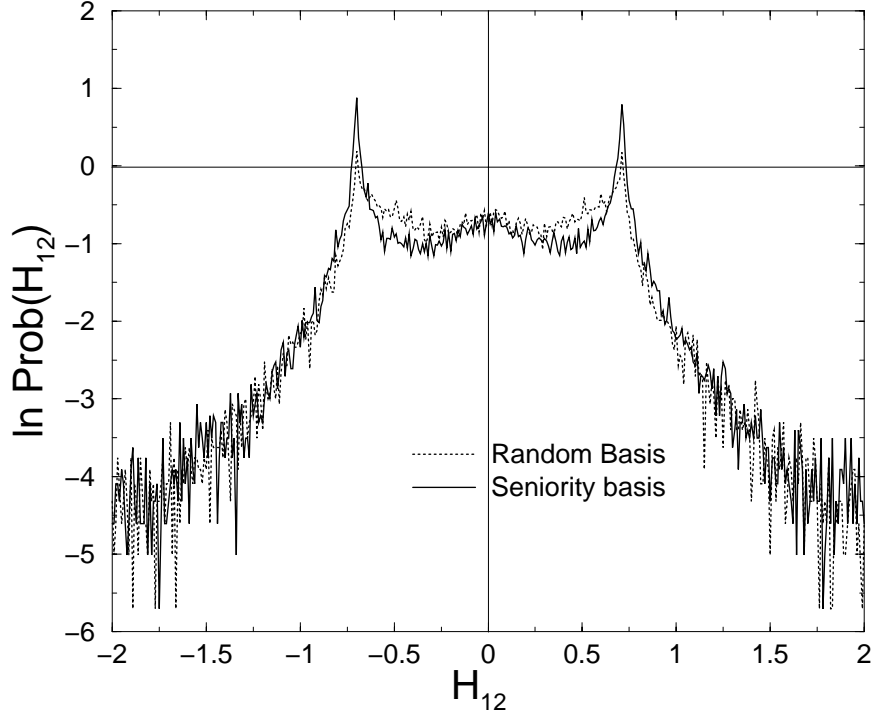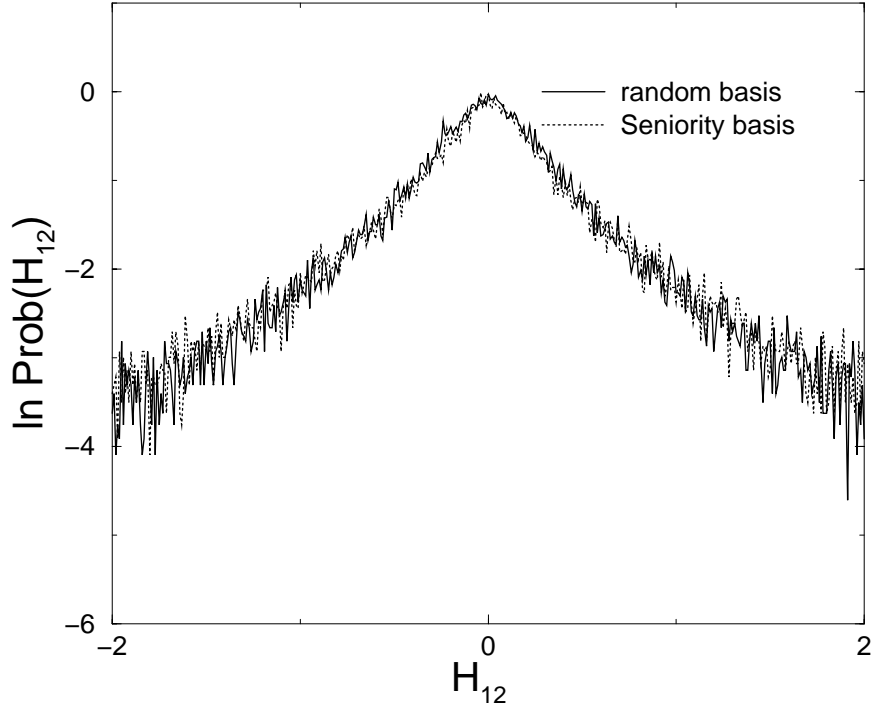
Figure 3.18: The probability distribution $P(H_{ij})$ of the off-diagonal matrix elements of the 2×2 $J = 0$ block of the $N = 4$, $j = 11/2$ Hamiltonian in the $|JM\rangle$ basis but this time rescaled with an alternative prescription to that of Fig. 3.17.

is especially true of the $N = 6$ systems. An obvious interpretation of this is that a state can have either one nature or another, but seldom combination of both.

Another geometric effect is that the pairs $\{S_{Q;4}[0], S_4[0]\}$ form an ellipse, see Fig. 3.21. This is to be expected as the $J = 0$ block is two dimensional, and the operators $\sum_\Lambda Q_{4\Lambda} Q_{4\Lambda}^\dagger$, and $\sum_\kappa M_{4\kappa} M_{4\kappa}^\dagger$ have different eigenvalues and eigenvectors. If we take the two eigenvectors of $\sum_\kappa M_{4\kappa} M_{4\kappa}^\dagger$ as a basis, and call the corresponding eigenvalues $M1$ and $M2$, any spin zero state of the system can be specified by an angle θ in this space. The eigenvectors of $\sum_\Lambda Q_{4\Lambda} Q_{4\Lambda}^\dagger$ make an angle ϕ with the axes, and have eigenvalues $Q1$ and $Q2$, now the pairs $\{S_{Q;4}[0], S_4[0]\}$ are just $\{ M1 \cos^2(\theta) + M2 \sin^2(\theta), Q1 \cos^2(\theta - \phi) + Q2 \sin^2(\theta - \phi)\}$, which is the equation for an ellipse parameterized by θ. The distribution of points $\{S_{Q;4}[2], S_4[2]\}$ can be explained by a similar argument for three dimensions as there are three $J = 2$ states again see Fig. 3.21. One must exercise extreme caution when

54
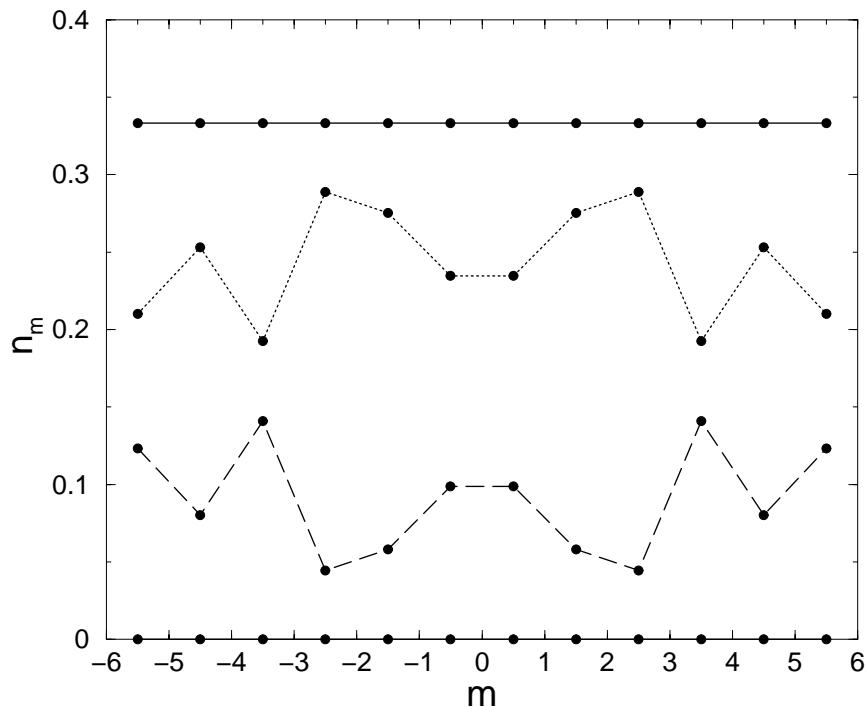
Figure 3.19: The contribution to the occupation numbers n_m of the $|S = 0, N = 4\rangle$ state from Slater determinants of seniority 0, straight line. The jagged lines depict the decomposition of n_m for $|S = 4, N = 4\rangle$ into contributions from seniority-4 (upper dotted line) and seniority-0 (lower dashed line) Slater determinants; here $j = 11/2$.

interpreting combinations of single-particle operators. There can be striking correlations begging to be misinterpreted as exciting physics instead of the subtle geometric effects that they so often are.

3.3.8 Pairing and fractional pair transfer collectivity

Previous investigators [11], [12], tried to pinpoint the role of pairing in this problem in a number of ways. So far we have seen that the pairing component of the random interaction, in the sense of the magnitude and sign of V_0, plays a minimal role. When set to 0 it doesn't impact the fraction of spectra with spin 0 ground states, Fig. 3.6(c). Furthermore the ground state wave functions are close to the chaotic limit, they are not oriented in the Hilbert space along the vector of the pure pairing wave function, Fig. 3.7. Following the example of
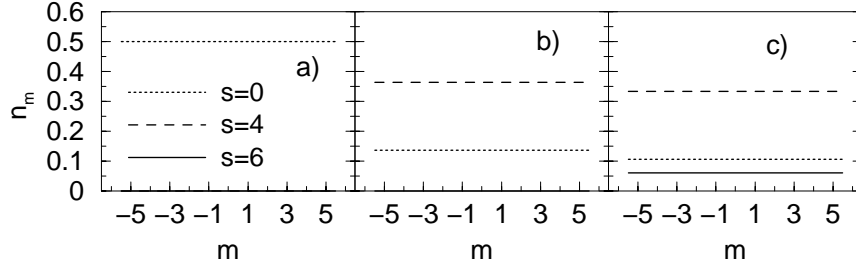
Figure 3.20: The contribution to n_m for the states $S = 0$, $N = 6$ (a), $S = 4$, $N = 6$ (b) and $S = 6$, $N = 6$ (c) from Slater determinants of various seniority; here $j = 11/2$. Note that for $J = 0$, n_m is independent of m.

Ref.[11], [?], we examine f_p, the so-called fractional pair transfer collectivity. f_p is defined by

$$f_p = \frac{\langle N-2|P_0|N\rangle^2}{\langle N|P_0^\dagger P_0|N\rangle}. \qquad (3.31)$$

The states $|N\rangle$ and $|N+2\rangle$ are spin zero ground states of N and $N+2$ particle systems with the same interaction parameters V_L, and single-particle spin j. The numerator is a measure of the extent that $|N+2\rangle$ is built by adding a spin zero pair to $|N\rangle$. The denominator counts the number of spin zero pairs in $|N\rangle$. A significant pairing interaction would favor a high degree of pairing in the ground state, making the distribution of f_p peaked at 1, and it is. This was interpreted as a signature of pairing. However a plot of $\langle N-2|P_0|N\rangle^2$ vs $\langle N|P_0^\dagger P_0|N\rangle$ reveals an interesting structure which may be a purely geometric effect, see Fig. 3.22. The structure is unaffected by setting $V_0 = 0$. In Fig. 3.22, the pair creation operator $P_0^\dagger$ connects the spin zero multiplets of the $N = 4$ and 6 particles which have dimensions 2 and 3 respectively. Conversely one can examine the opposite case, connecting the 6 particle state to a 4 particle state by the action of P_0 (which would leave the numerator unchanged in (3.31) but the denominator would then be $\langle 6|P_0^\dagger P_0|6\rangle$. In this case the structure in Fig. 3.22 is only slightly modified.

This can be explained by the geometric properties of $P_0^\dagger$ which are summarized in (3.17).
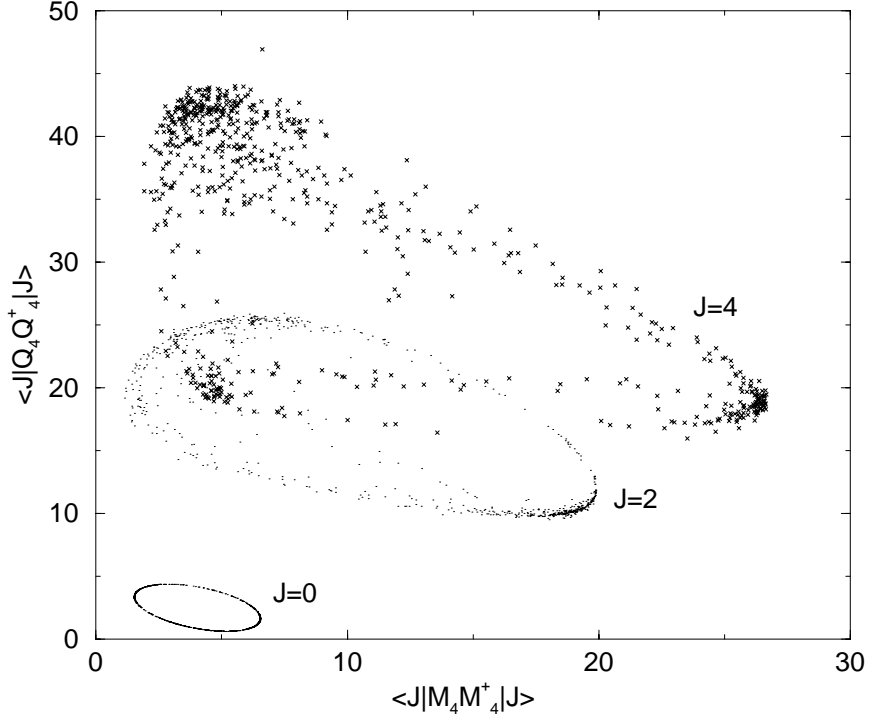
Figure 3.21: The quantities $S_{Q;L}[J]$ and $S_L[J]$ are strongly correlated for different values of J. This is just a geometric effect. The quantities are calculated for the lowest J states. Here $N = 4$ and $j = 11/2$.

Writing the general $N = 4$, 6 spin-zero states $|0\rangle_4$ and $|0\rangle_6$ in the seniority basis, $|S,N\rangle$, as $(\alpha|0,4\rangle + \beta|4,4\rangle)$, and $(\gamma|0,6\rangle + \delta|4,6\rangle + \gamma|6,6\rangle)$, with the additional constraint that $\alpha^2 + \beta^2 = 1$, and $\gamma^2 + \delta^2 + \varepsilon^2 = 1$, the plot Fig. 3.22 is the set of points

$$\{ {}_6\langle 0 | P_0^\dagger | 0 \rangle_4 = 10\alpha^2 + 2\gamma^2 \ , \ {}_4\langle 0 | P_0^\dagger P_0 | 0 \rangle_4 = 10\alpha^2 + 2 \}. \tag{3.32}$$

Note that for convenience we used $P_0^\dagger P_0$ ($= P_0 P_0^\dagger + 2$) instead of $P_0 P_0^\dagger$. The operator P_0 cannot connect $|6,6\rangle$ to $|4,4\rangle$ so the value of ε is either 0 or 1, which accounts for the points on the horizontal axis in Fig. 3.22. The straight line portion of the plot corresponds to $\alpha = \gamma$. In principle if α and γ are uncorrelated, the points would cover an area on the plane. The states $|0\rangle_4$ and $|0\rangle_{6,\varepsilon=0}$ make angles θ_4 and θ_6 in their respective two-dimensional planes. These angles were extracted from the wave functions and plotted against each other and are highly correlated (as too are α and γ), lying on a tangent to and on the positive side of the line $\theta_4 = \theta_6$, see Fig. 3.24. When this curve is rotated by $\frac{\pi}{2}$ so

57

as to lie tangent to the horizontal axis, it is, to a very high degree of accuracy, described by $A + B\cos(\omega\theta_4 + c)$ where $A = 0.0970$, $B = 0.1028$, $c = 0.8901\frac{\Pi}{2}$ and $\omega = 2.8288$. The reason for these phenomena, although qualitatively unexplained, are certainly geometric in nature.
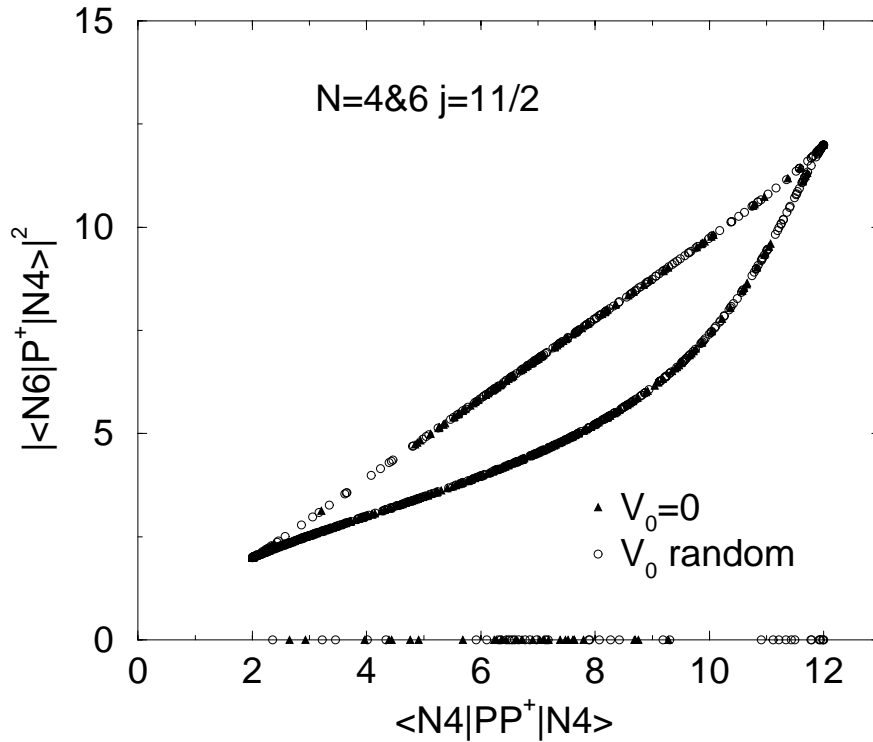
Figure 3.22: The numerator of f_p vs the denominator in eq. (3.31), evaluated for the $N = 4$

and 6, $j = 11/2$ systems with $J_0 = 0$. $P_0^\dagger$ creates a pair of particles coupled to spin zero. It acts on $N = 4$, $J = 0$ ground states to make an $N = 6$, $J = 0$ state which is overlapped with the ground state of the corresponding $N = 6$ system. The operator $P_0^\dagger P_0$ counts the number of pairs in the $N = 4$ state. Note the structure is unchanged by setting $V_L = 0$, again the effect is geometric.
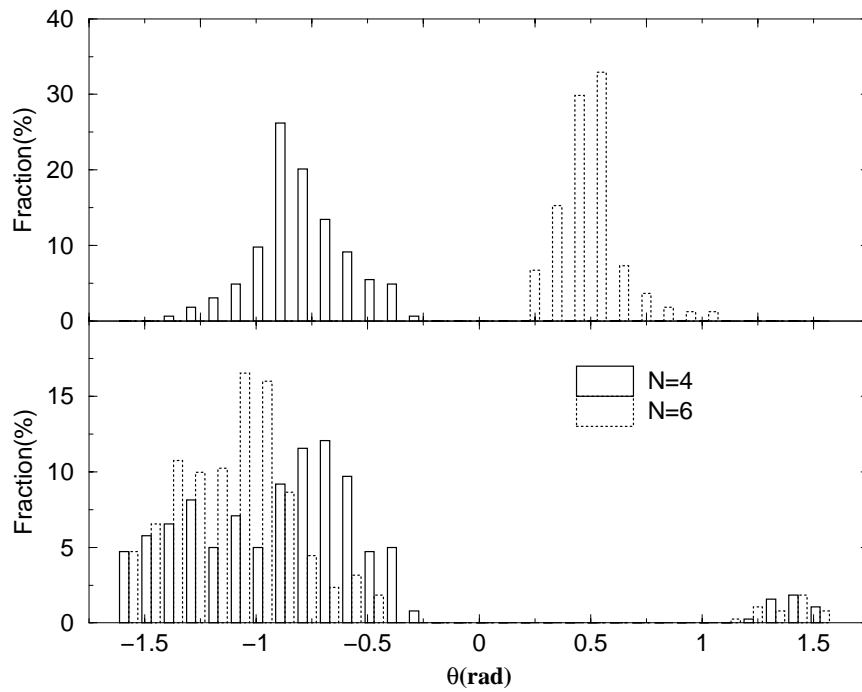
Figure 3.23: The distribution of the angles made by the $J = 0$ g.s. in the 2-dimensional space $\{|S = 0\rangle, |S = 4\rangle\}$ for $N = 4, 6$. Panel a) corresponds to those points on the straight line portion of Fig. 3.22 while panel b) is for those points on the curved part.
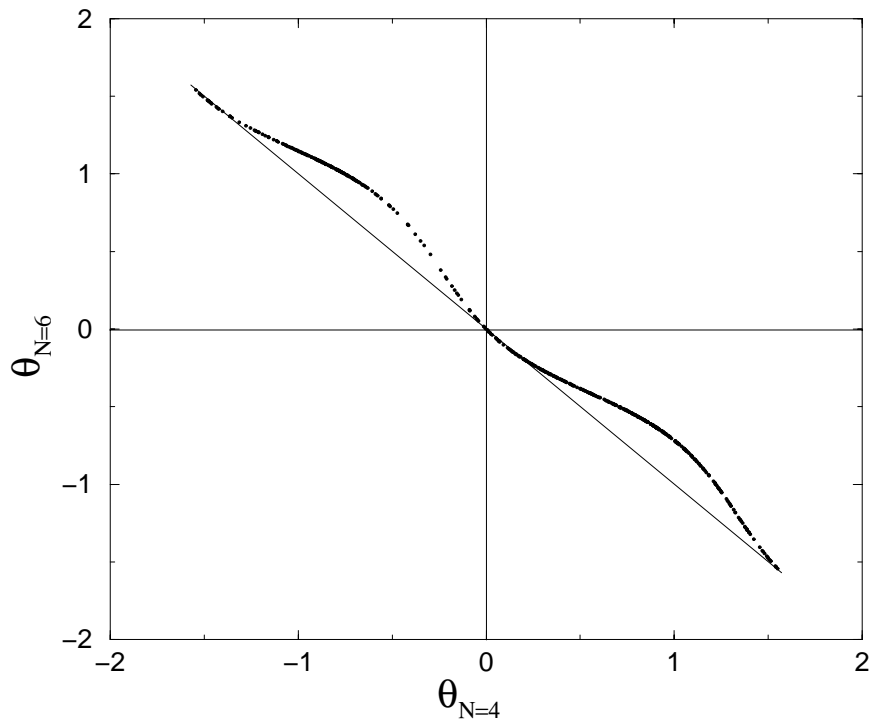
Figure 3.24: The strong correlation between the angle the spin-0 ground states make in the two-dimensional $N = 4$, $J = 0$ subspace, $\theta_{N=4}$ and $N = 6$, $J = 0$ subspace, $\theta_{N=6}$. The states are eigenstates of Hamiltonians with the same interaction parameters.

Chapter 4

A Statistical Theory

The high incidence of $J = 0$ and $J = J_{max}$ ground states can be thought of as a result of geometric chaoticity, i.e. the inherent complexity of an N-body system with fixed J. This feature depends only weakly on the ensemble from which the random Hamiltonians are taken, depending only on the geometry of the Hilbert space of the system. In other words the effect is determined by the Fermi-statistics of the particles, and the values of N and j. In the first illustrative example in Section (3.1), the analog of Hund's rule in atomic physics, the geometric factors of the system, $\mathbf{S}$ and $s(s+1)$, have been separated from the details of the interaction, i.e. the random number A, in a very simple way. We will approximately achieve a similar separation in our problem for the equilibrium energy of a state of angular momentum J. The role of A will be replaced by a relatively simple function of N and j, resulting from the geometric properties of the finite Fermi-system.

4.1   The Bosonic Approximation

One simple idea is related to the approximate realization of fermion pairs as bosons. The term beyond the boson-like commutator in (3.4) is of order $\frac{N}{\Omega}$. Here $\Omega = 2j + 1$ is the number of single-particle states, and N is the number of particles, so this term is small for small mean occupancies. Particle-hole conjugation means its analog will be small for

near full occupation also. For intermediate occupation it is not small but almost constant. This constant can be absorbed into $P_{L\Lambda}$ and $P^{\dagger}_{L'\Lambda'}$ by renormalizing them to get the nearly bosonic operators $b_{L\Lambda}$ and $b^{\dagger}_{L'\Lambda'}$. These 'bosons' are pairs of fermions, and their number and spin depend on the system (i.e. the set V_L). This simplifies the problem immensely. Now our Hamiltonian is a sum of random energies, ω_L, each of which are proportional to V_L.

$$H = \sum_{L\Lambda} V_L P^{\dagger}_{L\Lambda} P_{L\Lambda} = \sum_{L\Lambda} \omega_L n_L, \tag{4.1}$$

where n_L is the number operator of the bosons with spin-L. In each realization of the system, the fermion pairs form bosons which condense into the level with lowest energy, ie. the lowest ω_L. Once this happens, the total angular momentum J can be anywhere from 0 to $n_b L$ where n_b is the number of bosons. We see that already $L = 0$ is singled out, because in this case the only value J can have is 0, and this will happen $\frac{1}{k}$ of the time, where $k = j + 1/2$ is the number of values of L. For all other values, $J = 0$ accounts for a small fraction of the total space.

In short the bosonic approximation singles out $J = 0$ but doesn't account for the full effect. The values of $f_0 \sim 1/(j+1/2)$ are much lower than the observed values, and the j behavior is wrong compared with that seen in, for example, Fig. 3.1. Also, J_{max} is not singled out, and its allowed value is too high. See Fig. 4.1.

4.2   Equilibrium Statistical Mechanics Approach

Our approach is based on equilibrium statistical mechanics which, in the case of degenerate fermionic states, leads to the Fermi-Dirac distribution. The mean particle number with projection m on an arbitrary quantization axis is

$$n_m = \frac{1}{\exp(\gamma m - \mu) + 1}, \tag{4.2}$$
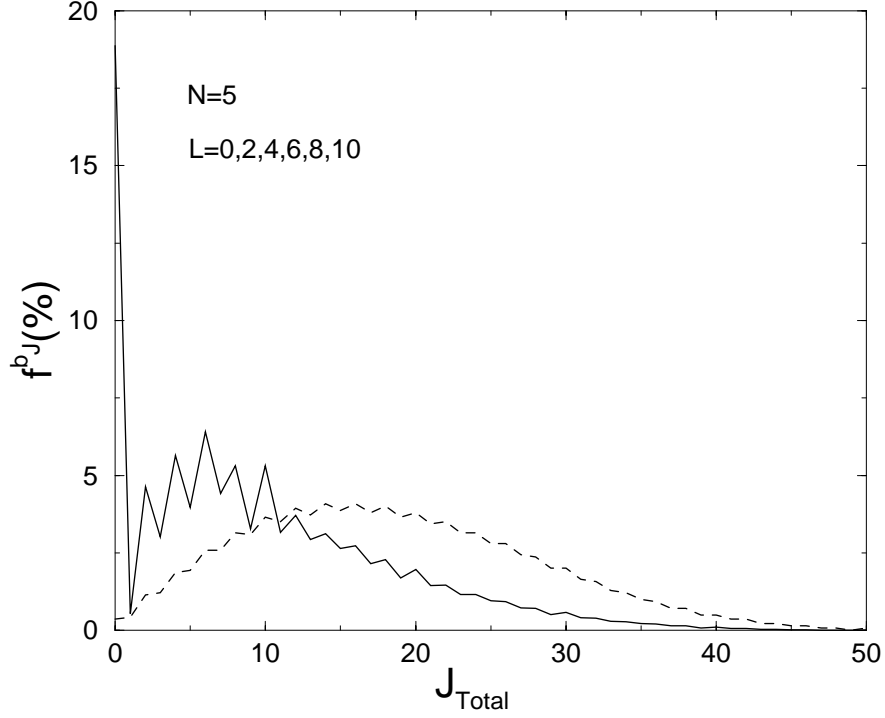
Figure 4.1: f_J^b for the bosonic approximation. The situation for $N = 6$, $j = 11/2$, is shown. Here $L_{max} = 10$, $k = 6$. The bosonic approximation gives the solid line while the statistical distribution of of allowed values of total angular momentum J, gives the dashed line. Note that f_0 only slightly exceeds $1/6$.

under the constraints for total particle number N and total angular momentum projection M,

$$N = \sum_m n_m, \quad M = \sum_m m n_m.$$ (4.3)

The quantization axis will later be identified with the total angular momentum J. It is reasonable to write this equation down and just start from there. However it can be derived from very general assumptions using the Darwin-Fowler method. A detailed derivation of this is included in Appendix (6.1). The quantities $\mu(N,M)$, the chemical potential, and $\gamma(N,M)$, the cranking frequency, are the Lagrange multipliers associated with the two constraints. The equilibrium energy for an N particle state with total projection M is

$$\langle H \rangle = \frac{1}{2} \sum_{L,\Lambda,1,2,3,4} V_L C_{12}^{L\Lambda} C_{43}^{L\Lambda} \langle a_1^\dagger a_2^\dagger a_3 a_4 \rangle,$$ (4.4)

63

where as before $C_{12}^{L\Lambda}$ is the Clebsch-Gordan coefficient $\langle L,\Lambda|j,m_1;j,m_2\rangle$. The assumption of statistical equilibrium implies the off-diagonal matrix elements of a_m and $a_m^\dagger$ and their products make an incoherent contribution to the expectation value which sums to zero. We introduce another approximation at this point by treating the single-particle occupation numbers as uncorrelated, $\langle n_1 n_2\rangle \to \langle n_1\rangle\langle n_2\rangle$. This is a key approximation and is based on the assumption of quantum chaos, where the eigenstates are chaotic. Keeping N fixed, and using the commutation rules for a_m and $a_m^\dagger$, (4.4) can be rewritten as

$$\langle H\rangle = \sum_{L,\Lambda,1,2} V_L \left|C_{12}^{L\Lambda}\right|^2 \langle n_1\rangle\langle n_2\rangle, \tag{4.5}$$

For $M=0$ the single-particle occupancies n_m are uniform,

$$n_0 = \frac{1}{1+e^{-\mu_0}} = \frac{N}{\Omega} \quad , \quad (\Omega = 2j+1) \tag{4.6}$$

where $\mu_0 = \mu(N, M=0)$. For $M \neq 0$ and treating γ as an expansion parameter,

$$n_m = \frac{1}{1+e^{-\mu+\gamma m}} = \frac{1}{1+e^{-\mu}}(1 - \alpha(\gamma m + \frac{1}{2}\gamma^2 m^2) + \alpha^2\gamma^2 m^2). \tag{4.7}$$

Here

$$\alpha = \frac{e^{-\mu}}{1+e^{-\mu}}. \tag{4.8}$$

Expanding the chemical potential, $\mu(N,M) = \mu_0 + \Delta\mu$ and using the constraint $N = \sum_m n_m$ we get

$$\mu(N,M) = \mu_0 + (\alpha_0 - \frac{1}{2})\gamma^2\langle m^2\rangle + O(\gamma^4). \tag{4.9}$$

The final expression for n_m is

$$n_m = \frac{1}{1+e^{-\mu_0}}[1-\alpha_0\gamma m+$$

$$\alpha_0(\alpha_0-\frac{1}{2})(m^2-\langle m^2\rangle)\gamma^2 \qquad (4.10)$$

$$+\alpha_0((2\alpha_0-1)(\alpha_0-\frac{1}{2})\langle m^2\rangle m$$

$$-(\alpha_0^2-\alpha_0+\frac{1}{6})m^3)\gamma^3$$

$$+\alpha_0(\alpha_0-\frac{1}{2})((\alpha_0^2-\alpha_0+\frac{1}{12})(m^4-\langle m^4\rangle)$$

$$-(3\alpha_0^2-3\alpha_0+\frac{1}{2})\langle m^2\rangle(\langle m^2\rangle-m^2))\gamma^4].$$

$$(4.11)$$

where

$$\alpha_0 = \frac{e^{-\mu_0}}{1+e^{-\mu_0}} = \frac{\Omega-N}{\Omega} = 1-n_0. \qquad (4.12)$$

Thus the equilibrium energy for a state with N particles and total projection M is

$$\langle H\rangle_{N,M} = \sum_{L,\Lambda,1,2} V_L\left|C_{12}^{L\Lambda}\right|^2(\frac{N}{\Omega})^2[1+$$

$$\alpha_0^2\gamma^2 m_1 m_2 + \alpha_0(\alpha_0-\frac{1}{2})(m_1^2+m_2^2-2\langle m^2\rangle)\gamma^2$$

$$-\alpha_0^2[(2\alpha_0-1)(\alpha_0-\frac{1}{2})\langle m^2\rangle(m_1 m_2+m_2 m_1)-$$

$$(\alpha_0^2-\alpha_0+\frac{1}{6})(m_1 m_2^3+m_2 m_1^3)]\gamma^4$$

$$+\alpha_0(\alpha_0-\frac{1}{2})[(\alpha_0^2-\alpha_0+\frac{1}{12})(m_1^4+m_2^4-2\langle m^4\rangle)-$$

$$(3\alpha_0^2-3\alpha_0+\frac{1}{2})\langle m^2\rangle(2\langle m^2\rangle-m_1^2-m_2^2)\gamma^4]. \qquad (4.13)$$

We use $M=\sum_m mn_m$ to replace γ to get

$$\gamma(N,M) = -\frac{M}{N\alpha_0\langle m^2\rangle} = -\frac{3M}{(\Omega-N)j(j+1)}. \qquad (4.14)$$

It is important to note that γ is treated as an expansion parameter, so this procedure is not good for all values of γ. However it is valid for a wide range as seen in Fig. 4.2. Finally,

after using the explicit values for the sums, see Appendix (6.2), all this fits together to give

$$\langle H \rangle_{NM} = \frac{N^2}{\Omega^2} \sum_L (2L+1) V_L \tag{4.15}$$

$$+ M^2 \frac{3}{2\mathbf{j}^4 \Omega^2} \sum_L (2L+1) V_L \left(\mathbf{L}^2 - 2\mathbf{j}^2 \right)$$

$$+ M^4 \frac{9 \left(\Omega - 2N \right)^2}{40 \mathbf{j}^8 \left(\Omega - N \right)^2 N^2 \Omega^2} \sum_L (2L+1) V_L$$
$$\times \left(3\mathbf{L}^4 + 3\mathbf{L}^2 - 12\mathbf{j}^2 \mathbf{L}^2 - 6\mathbf{j}^2 + 8\mathbf{j}^4 \right) .$$
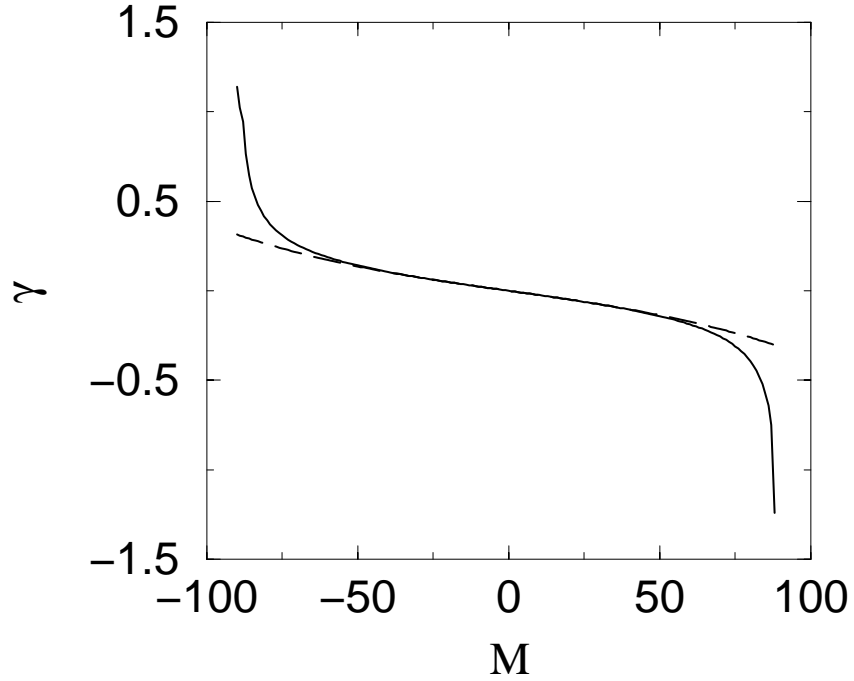
Figure 4.2: The cranking frequency γ vs. M for N=10 and j=27/2. Solid and dotted lines correspond to exact and approximate values, respectively. This gives an indication of the range of validity of the expansion that gives eq. (4.14).

Identifying $\langle H \rangle_{N,J}$ with $\langle H \rangle_{N,M=J}$ we have the main result of the statistical treatment,

$$\langle H \rangle_{N,J} = \sum_L (2L+1) V_L \left(h_0(L) + h_2(L) J^2 + h_4(L) J^4 \right), \tag{4.16}$$

where

$$h_0(L) = \frac{N^2}{\Omega^2},$$

$$h_2(L) = \frac{3}{2\mathbf{j}^4\Omega^2}(\mathbf{L}^2 - 2\mathbf{j}^2),$$

$$h_4(L) = \frac{9(\Omega - 2N)^2}{40\mathbf{j}^8(\Omega - N)^2 N^2 \Omega^2}$$

$$\times \left(3\mathbf{L}^4 + 3\mathbf{L}^2 - 12\mathbf{j}^2\mathbf{L}^2 - 6\mathbf{j}^2 + 8\mathbf{j}^4\right). \tag{4.17}$$

Note that the J^2 term in (4.16) can be written down directly from the $K = 1$ term in eq. (3.6) as an effective spin-spin interaction i the particle-hole channel,

$$\tilde{V}_1 = 3 \sum_{L\,\text{even}} (2L+1) \begin{Bmatrix} j & j & 1 \\ j & j & L \end{Bmatrix} V_L. \tag{4.18}$$

with

$$\begin{Bmatrix} j & j & 1 \\ j & j & L \end{Bmatrix} = \frac{\mathbf{L}^2 - 2\mathbf{j}^2}{\Omega 2\mathbf{j}^2} \tag{4.19}$$

4.3 Ground State Spin

Given that the regular features of the spectra are independent of the choice of ensemble, the distribution of equilibrium energies (4.16) can be evaluated analytically assuming a Gaussian distribution for each interaction strength V_L

$$P_L(V_L) = \frac{1}{\sqrt{2\pi\sigma_L^2}} \exp\left(-\frac{(V_L - \langle V_L \rangle)^2}{2\sigma_L^2}\right). \tag{4.20}$$

Our Hamiltonian in Eq. (4.16) has a form

$$\langle H \rangle = \text{const} + aJ^2 + bJ^4, \tag{4.21}$$

where

$$a = \sum_L V_L a_L, \quad b = \sum_L V_L b_L, \tag{4.22}$$

67

and

$$a_L = \frac{3}{2\mathbf{j}^4\Omega^2}(2L+1)(\mathbf{L}^2-2\mathbf{j}^2),\tag{4.23}$$

$$b_L = \frac{9(\Omega-2N)^2}{40\mathbf{j}^8(\Omega-N)^2N^2\Omega^2}(2L+1)(3\mathbf{L}^4+3\mathbf{L}^2-12\mathbf{j}^2\mathbf{L}^2-6\mathbf{j}^2+8\mathbf{j}^4),$$

We will first examine the probability that this random system has given values of a and b. This is given by

$$P(a,b) = \int \delta\left(a-\sum_L V_L a_L\right)\delta\left(b-\sum_L V_L b_L\right)\prod_L P_L(V_L)\,dV_L.\tag{4.24}$$

This can be rewritten by using the Fourier representation of the delta function, $\delta(x) = \int \frac{e^{i\lambda x}}{2\pi}d\lambda$ and performing all integrals over V_L to get

$$P(a,b) = \frac{1}{4\pi^2}\int d\lambda\,d\lambda'\,e^{i\lambda a+i\lambda'b}\tag{4.25}$$

$$\times \prod_L\exp\left(-\frac{1}{2}\sum_L(\lambda a_L+\lambda'b_L)^2\sigma_L^2 - i\sum_L\langle V_L\rangle(\lambda a_L+\lambda'b_L)\right).$$

The remaining two dimensional Gaussian integral over λ and λ' is again relatively easy,

$$P(a,b) = \frac{1}{2\pi\sqrt{AB-D^2}}\exp\left(-\frac{B\xi_a^2-2D\xi_a\xi_b+A\xi_b^2}{2(AB-D^2)}\right),\tag{4.26}$$

where we have defined

$$A = \sum_L a_L^2\sigma_L^2,\quad B = \sum_L b_L^2\sigma_L^2,\qquad D = \sum_L a_L b_L\sigma_L^2,\tag{4.27}$$

and

$$\xi_a = a-\sum_L\langle V_L\rangle a_L,\qquad \xi_b = b-\sum_L\langle V_L\rangle b_L.\tag{4.28}$$

Assuming $\langle V_L\rangle = 0$ we have

$$P(a,b) = \frac{1}{2\pi\sqrt{AB-D^2}}\exp\left(-\frac{Ba^2-2Dab+Ab^2}{2(AB-D^2)}\right).\tag{4.29}$$

68

This is a two dimensional Gaussian distribution, the independent distribution of one variable is also Gaussian

$$P(a) = \int db P(a,b) = \frac{1}{\sqrt{2\pi A}} e^{-a^2/2A}.$$ (4.30)

We first address the question of the probability that the ground state has spin zero. The $a \geq 0$ in Eq. (4.21) is an obvious necessary condition, and if $b > 0$ the statement is definitely true. In the case $b < 0$ the curve $\langle H \rangle$ eventually goes down and there is a possibility to have a ground state at the maximum possible value of $J_{\max} = (j - (N-1)/2)N$. Finally the condition for the zero ground state can be expressed as $a \geq 0$ and $a + bJ_{\max}^2 > 0$. The probability of the ground state having spin zero is given by the integral over the region

$$P = \int_{a \geq 0, b > -a/J_{\max}^2} P(a,b) \, da \, db.$$ (4.31)

In spherical coordinates $a = r \cos \phi$ and $b = r \sin \phi$ the region of integration is

$$\phi \in [-\arctan(1/J_{\max}^2), \pi/2],$$ (4.32)

which gives

$$P = \frac{1}{4} + \frac{1}{2\pi} \arctan \left[\frac{D + A/J_{\max}^2}{\sqrt{AB - D^2}} \right].$$ (4.33)

Fig. 4.3 (top panels), dashed line, shows the smooth behavior of the probability f_0 as a function of j for $N = 4$, and 6 particles. The solid line gives the results of the exact numerical diagonalization. This simple statistical theory captures the excess of $J = 0$ ground states but of course it does not explain the observed staggering effects.

It would be premature to conclude from (4.16) that the remaining 50% of cases have a maximum spin ground state. Indeed, the expansion used for γ in the derivation is not valid for large angular momenta. However, the wave functions for the largest possible spins are unique and can be constructed explicitly being independent of the interaction parameters. Their energies can be compared to the energies of lower spins. In this a slight improvement
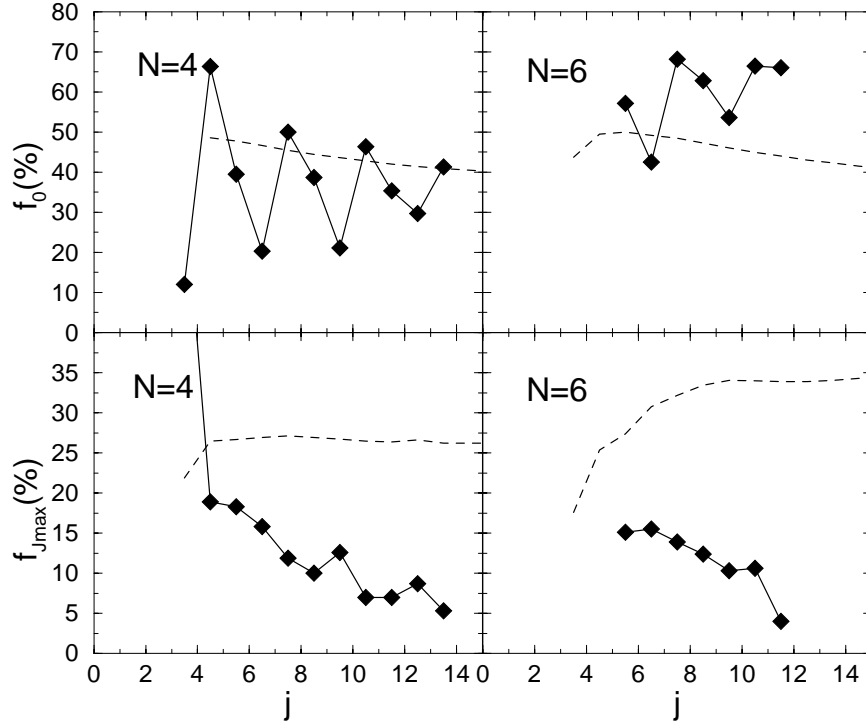
Figure 4.3: f_0, the fraction of ground states with $J = 0$, and (an upper boundary for) $f_{J_{max}}$ for $N = 4$, and 6 for different j. Ensemble results; solid line. Statistical theory; dotted line.

in the results is obtained above for spin f_0 (this is taken into account in plotting Fig. 4.3), and we also extract the upper boundary for the probability of the maximum ground state spin J_{max}, Fig. 4.3, (lower panels).

Thus, the statistical approach provides a natural qualitative explanation and reasonable quantitative estimate for the dominance of ground states spins $J_0 = 0$ and $J_0 = J_{max}$ in our ensemble. Other non-statistical details of the picture, especially the non-monotonous changes like the odd-even staggering of f_0, require a more subtle approach.

4.4 The Distribution of V_L for $J_0 = J_{max}$

The spin of the ground state in each particular realization is determined by the values of V_L in this realization. The subset of V_L that gives $J_0 = 0$ or $J_0 = J_{max}$ has been discussed in section 3.3.4. We can use (4.16) to calculate the mean values $\langle V_L \rangle$ of those subsets that give

$J_0 = J_{max}$. If we assume that the V_L's have a Gaussian distribution this can be achieved by exact integration. In Fig. 4.4 the theoretical values for $\langle V_L \rangle$ vs. L were compared with the mean values of actual sets of random parameters V_L which led to $J_0 = J_{max}$. The resulting curve is in total agreement with the statistical theory.
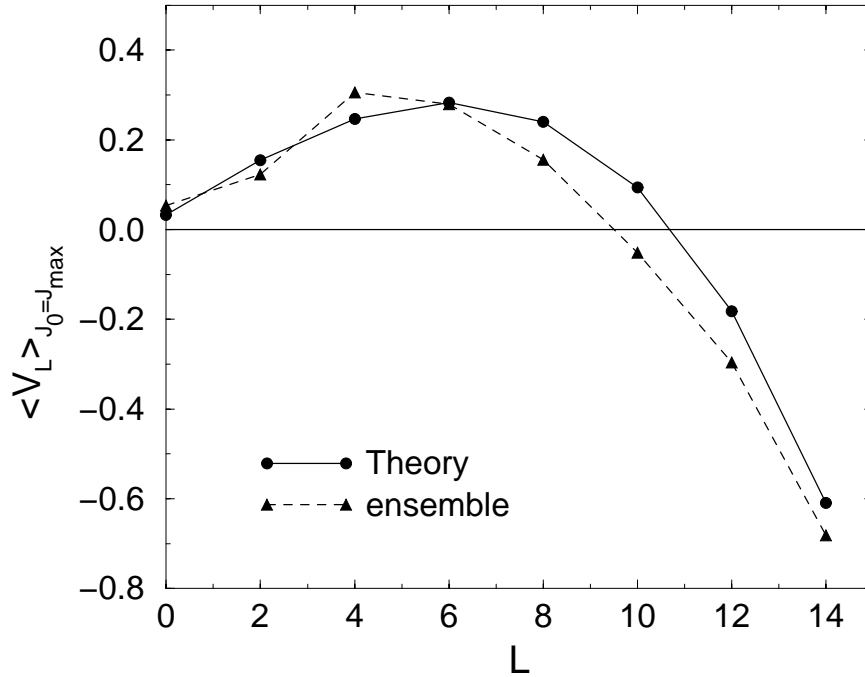
Figure 4.4: The mean values of V_L for the subsets of V_L that result in $J_0 = J_{max}$ ground states. The theory, solid line, agrees with the ensemble average values, dashed line. Here $N = 4$ and $j = \frac{15}{2}$.

4.5 Ground State Energy

The equilibrium energies (4.16) are strongly correlated with the corresponding numerical values. In a scatter plot of theoretical energies vs numerical energies for a specific value of J, the points fall about a straight line, as in Fig. 4.5. Two subsets of the spectra were selected, those with $J_0 = 0$ and $J_0 = J_{max}$. The slopes of the lines were independent of J in both groups, having a value of 0.81 ± 0.03. This is a direct result of treating the single-particle occupation numbers n_m as uncorrelated. When the exact correlated occupancies

are used to evaluate (4.5) the slopes become 0.98 ± 0.03. The theoretical energies for a given ensemble are shifted by a constant negative amount that decreases with J, as in Fig. 4.6. The shift was smaller for the $J_0 = J_{max}$ set. Using the correlated occupation numbers only reduced the magnitude of the shift by 15%. This nonstatistical effect is presumably due to the regular part of the dynamics related to $\langle V_L^2 \rangle$. The simplest description of this part can be reached with the aid of the boson expansion technique [4], and corresponds in fact to boson pairing. For $J_0 = J_{max}$, Fig. 4.5(b), the ground state energy (??) is in one-to-one correspondence to the statistical predictions, although the slope differs slightly from unity because of the use of the γ-expansion.
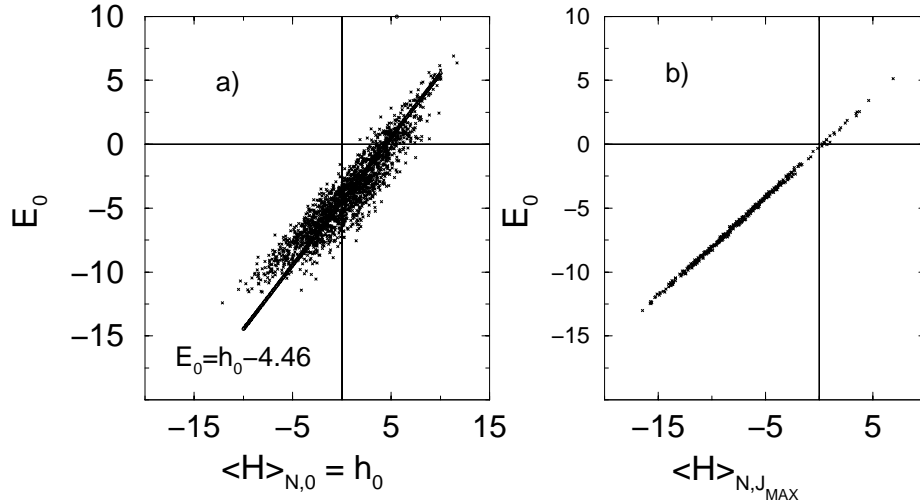
Figure 4.5: Ground state energies E_0 for $J_0 = 0$,(a), and $J_0 = J_{max}$,(b), vs. predictions of the statistical model, eq. (4.16). Here $N = 6$ and $j = 17/2$. The theoretical energies are fit to a straight line, included in (a).

4.6 Single-Particle Occupation Numbers

The single-particle occupation numbers n_m can be written in terms of the multipole operators using (3.7) as

$$a_m^\dagger a_m = \sum_K C_{jm\ j-m}^{K0} (-)^{j+m} M_{K0}^\dagger, \tag{4.34}$$
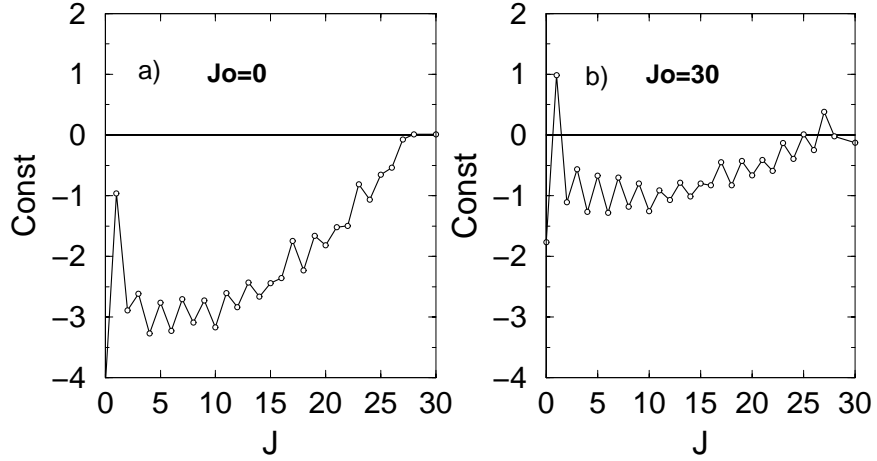
Figure 4.6: The constant shift in the theoretical equilibrium energies of spin J vs. J for the $N = 6$ $j = 15/2$ ensemble.

where $0 \leq K \leq 2j$. The average n_m oscillate about their theoretical values. These oscillations indicate a shell structure that is not captured by the statistical theory. This arises from the effective deformation present in individual realizations and requires a self consistent mean field approach. The occupation numbers exhibit an oscillatory behavior in Fig. 4.7, which may follow from the similarity of the Clebsch-Gordan coefficient $\langle K0 | jm, j-m \rangle$ and the Legendre polynomial $P_K(m/\sqrt{j(j+1)})$. In the Legendre polynomial expansion of n_m for a wave function $|J, J\rangle$ the coefficients of $P_K(x)$ are zero for $K > 2J$. In other words, the curves in Fig. 4.7 are precisely described by the first $2J + 1$ Legendre polynomials.

4.7 Moment of Inertia

The effective moment of inertia can be estimated directly from the rotational term of the equilibrium energy (4.16),

$$H_{rot} = A\mathbf{J}^2, \quad A = \frac{3}{4\Omega^2 \mathbf{j}^4} \sum_{L\,\text{even}} (2L+1)V_L(\mathbf{L}^2 - 2\mathbf{j}^2). \tag{4.35}$$

The contribution to the moment of inertia by the pair interaction for a pair with spin L changes its sign at $\mathbf{L}^2 = 2\mathbf{j}^2$, which corresponds to the absence of alignment of the paired
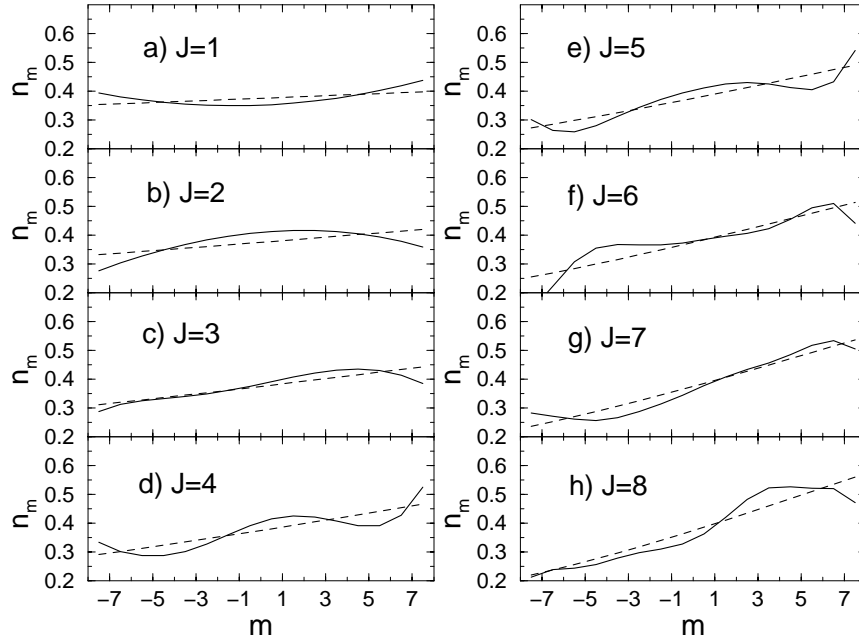
73

Figure 4.7: The single-particle occupation numbers n_m averaged over the lowest energy spin J wave functions of the 1417 out of 2000 (70%) spectra with $J_0 = 0$ (solid line), compared to the simplest theoretical expression (4.10) (dashed line)

particles, as their spins are perpendicular to each other. At low L pairs are antialigned, $\mathbf{L}^2 < 2\mathbf{j}^2$. If these pair states are attractive, $V_L < 0$, the contribution to the moment inertia is positive, preferring a normal rotational spectrum with angular momentum increasing with excitation energy. Contrary to that, at high L, the pairs are aligned, $\mathbf{L}^2 > 2\mathbf{j}^2$, so that the attraction in such pairs leads to the negative contribution to the moment of inertia which favors the bands with an inverted spin sequence. The moment of inertia was taken from the coefficient of J^2 in (4.35) via

$$I = \frac{1}{2A} \, , \tag{4.36}$$

and was nearly independent of N, in agreement with the statistical theory, Eq. (4.35). Again this implies non-collectivity. What I does depend on is geometry, in the guise of j. The calculated moment of inertia I is in excellent agreement with the ensemble results for $N = 4$ and 6 and all values of j, see Fig. 4.8.
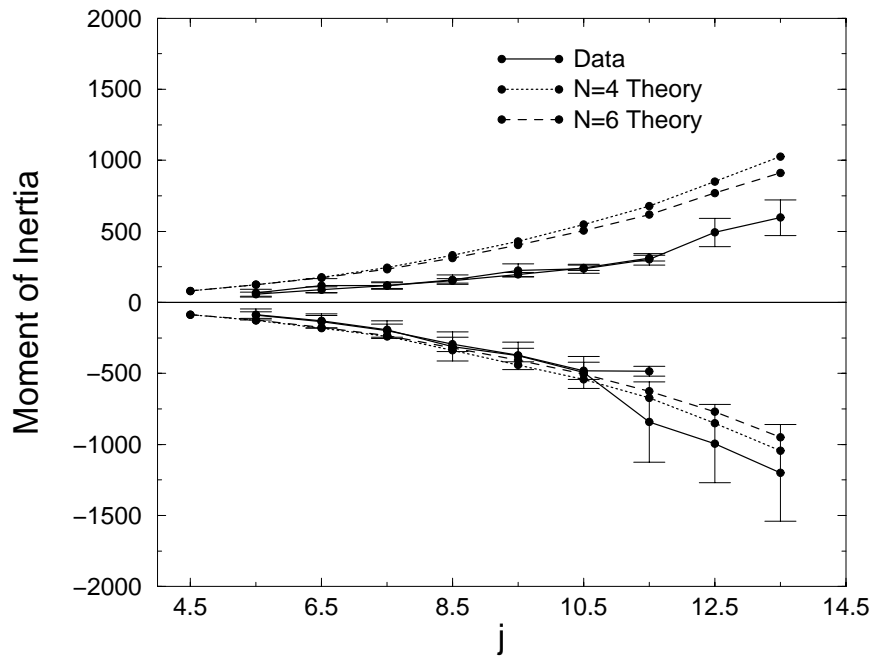
74

Figure 4.8: The moment of inertia for the $N = 4$ and 6 particle systems of a given j plotted as a function of j. The positive values are for the $J_0 = 0$ systems and the negative values correspond to the $J_0 = J_{max}$ systems.

Chapter 5

Conclusions

The main purpose of this dissertation is to shed light on the origin of the regularities in nuclear spectra, and the application of quantum chaos theory to nuclear spectra. In principle the results are also applicable to atomic systems, quantum dots, and other mesoscopic systems.

After some background on the theory of quantum chaos, a review of current research on this and related problems was presented. An analysis of neutron resonance data in the framework of Random Matrix Theory was described, where the problem of finding the relative fractions of resonances with a given spin was tackled. The results were mixed. Of the four sets of data analyzed, only the ^{235}U data yielded positive results. The level spacing distribution, the $\Delta_3(L)$ statistic, and the distribution of reduced widths all gave realistic values for this fraction. The problem is assumed to lie in the technical difficulties of taking high quality uncontaminated data.

Next the main problem of the dissertation was described and formulated. The regularities in nuclear spectra, especially the spin-zero ground states of even-even nuclei, are usually ascribed to the effect of the nuclear pairing interaction. While no-one doubts this, it is seen to be an incomplete picture in general. Regularities, similar to those in nuclear spectra, are seen in the spectra of random two-body Hamiltonians. The largely ignored role of

geometric chaoticity is shown to be the driving force behind this. Some simple illustrative examples of this mechanism are discussed, where the probability of the ground state spin for a simple system with a random spin-spin interaction is separated into a product of terms, one containing the random interaction parameter, and the other the geometric information, particle spin and particle number. This separation of the different aspects of the interaction is ultimately achieved for a more complicated system described in Chapter 3. A system of N spin-j fermions under the influence of a random two-body angular momentum conserving interaction was studied. The spectra exhibited many interesting features, the strongest of these was a propensity for the ground states to be magnetically aligned (maximum spin) or anti-aligned (spin-zero). The role of pairing, the V_0 parameter, was unambiguously eliminated as the culprit. A statistical theory based on equilibrium statistical mechanics was developed, and an expression for the equilibrium energy derived. The important point is that the equilibrium energy for the angular momentum-J state was expressed as a sum of products of two terms, one containing all the random interaction information, the other containing geometric information. The theory was used to successfully describe the salient features of the ensembles studied.

The conclusion of it all is that the previously ignored role of quantum chaos in shaping nuclear spectra dominates in systems of randomly interacting spectra. At the very least, quantum chaos cannot be dismissed in studies of the properties of nuclear spectra. Although this work was motivated by issues in nuclear spectroscopy, the theory was developed without specific reference to nuclear structure, only statistical mechanics. The results concern any small Fermi systems and can be applied to atomic systems, quantum dots, and other mesoscopic systems of condensed matter physics. For the first time in quantum many-body chaos correlations between blocks with different quantum numbers were shown to play an important role. This is a fresh angle on the theory of quantum chaos where the union between the chaotic structure of the eigenfunctions and the geometry of the finite

Fermi-system spawn regularity in the spectrum.

Chapter 6

Appendices

6.1 The Darwin-Fowler Method

This section details a derivation of Eq. (4.2) for the single-particle occupation numbers which is the foundation of the statistical theory of the text. The method is very elegant, and can be applied to get the density of levels labelled with *any additive* quantum number.

The goal is to get an expression for the number of states with angular momentum projection M, in a system of A *fermions*, each with spin J. Of course one can immediately write

$$\rho(A,M) = \sum_{n,i} \delta(A-n)\delta(M-M_i(n)) \tag{6.1}$$

where $M_i(n)$ is the ith possible value of M for an N-particle system. This expression is exact, but not at all useful as it stands. Let's take the Laplace transform of (6.1):

$$
\begin{aligned}
L\left[\rho(A,M)\right] &= \sum_{n,i}\int_0^\infty dA\int_0^\infty dM\exp(-M\lambda-A\mu)\,\delta(A-n)\,\delta(M-M_i(n)) \\
&= \sum_{n,i}e^{-M_i(n)\lambda-A\mu} \\
&= \prod_m(1+e^{-m\lambda-\mu}) \\
&= Z(\lambda,\mu) \tag{6.2}
\end{aligned}
$$

where *m* takes all possible values of the single-particle projection.

Now this is something one can handle, because taking the inverse Laplace transform gets us back to $\rho(A,M)$ but without the nasty δ-function (essentially all thats being done is using the Fourier representation of the δ-functions).

$$
\begin{aligned}
\rho(A,M) &= L^{-1}[Z(\lambda,\mu)] \\
&= \left(\frac{1}{2\pi i}\right)^2 \int_{-i\infty}^{i\infty} d\lambda \int_{-i\infty}^{i\infty} d\mu \, e^{M\lambda+A\mu} \prod_m (1+e^{-m\lambda-\mu}) \\
&= \left(\frac{1}{2\pi i}\right)^2 \int_{-i\infty}^{i\infty} d\lambda \int_{-i\infty}^{i\infty} d\mu \, e^{M\lambda+A\mu+\sum_m \ln(1+e^{-m\lambda-\mu})} \\
&= \left(\frac{1}{2\pi i}\right)^2 \int_{-i\infty}^{i\infty} d\lambda \int_{-i\infty}^{i\infty} d\mu \, e^{F(\lambda,\mu)}
\end{aligned}
\tag{6.3}
$$

where

$$
F(\lambda,\mu) = M\lambda + A\mu + \sum_m \ln(1+e^{-m\lambda-\mu}).
\tag{6.4}
$$

The saddle-point approximation can be used to evaluate this integral:

$$
\begin{aligned}
F(\lambda,\mu) &= F(\lambda_0,\mu_0) + (\lambda-\lambda_0)F_\lambda(\lambda_0,\mu_0) \\
&+ (\mu-\mu_0)F_\mu(\lambda_0,\mu_0) + \frac{1}{2}(\lambda-\lambda_0)^2 F_{\lambda\lambda}(\lambda_0,\mu_0) \\
&+ (\lambda-\lambda_0)(\mu-\mu_0)F_{\lambda\mu}(\lambda_0,\mu_0) + \frac{1}{2}(\mu-\mu_0)^2 F_{\mu\mu}(\lambda_0,\mu_0)
\end{aligned}
\tag{6.5}
$$

where the notation $F_\lambda(\lambda_0,\mu_0) = \frac{\partial}{\partial\lambda}F(\lambda,\mu)|_{\lambda_0,\mu_0}$ etc has been employed. The point (λ_0,μ_0) is the saddle-point, ie. $F_\lambda(\lambda_0,\mu_0) = F_\mu(\lambda_0,\mu_0) = 0$.

80

Straightforward differentiation gives the following set of equations:

$$F_\lambda(\lambda,\mu) = M - \sum_m \frac{m}{(1+e^{m\lambda+\mu})}$$

$$F_\mu(\lambda,\mu) = A - \sum_m \frac{1}{(1+e^{m\lambda+\mu})}$$

$$F_{\lambda\lambda}(\lambda,\mu) = \sum_m \frac{m^2\, e^{m\lambda+\mu}}{(1+e^{m\lambda+\mu})^2}$$

$$F_{\mu\mu}(\lambda,\mu) = \sum_m \frac{e^{m\lambda+\mu}}{(1+e^{m\lambda+\mu})^2}.$$

(6.6)

From the definition of the saddle-point we have

$$M = \sum_m \frac{m}{(1+e^{m\lambda_0+\mu_0})}$$

$$A = \sum_m \frac{1}{(1+e^{m\lambda_0+\mu_0})}.$$

(6.7)

which gives (4.2).

The following definitions clean up the notation a little;

$$f_0 = F(\lambda_0,\mu_0)$$

$$a = \frac{1}{2}\sum_m \frac{m^2\, e^{m\lambda_0+\mu_0}}{(1+e^{m\lambda_0+\mu_0})^2}$$

$$b = \frac{1}{2}\sum_m \frac{e^{\lambda_0+\mu_0}}{(1+e^{m\lambda_0+\mu_0})^2}$$

$$c = \sum_m \frac{m\, e^{m\lambda_0+\mu_0}}{(1+e^{m\lambda_0+\mu_0})^2}$$

(6.8)

Now we are left with

$$\rho(A,M) = \left(\frac{1}{2\pi i}\right)^2 \int_{-i\infty}^{i\infty} d\lambda \int_{-i\infty}^{i\infty} d\mu\, e^{f_0+a(\lambda-\lambda_0)^2+b(\mu-\mu_0)^2+c(\lambda-\lambda_0)(\mu-\mu_0)}.$$

81

Completing the square in the exponent and remembering that (6.7) give us $\lambda_0(A,M)$ and $\mu_0(A,M)$ we have the final result:

$$\rho(A,M) = \frac{e^{f_0(A,M)}}{2\pi\sqrt{4a(A,M)b(A,M)-c(A,M)^2}}.$$
(6.9)

6.2 Sums Involving Clebsch-Gordan Coefficients

In order to evaluate sums like $\sum_{\Lambda,1,2}\left|C_{12}^{L\Lambda}\right|^2 m_1^p$ or $\sum_{\Lambda,1,2}\left|C_{12}^{L\Lambda}\right|^2 m_1^p m_2^q$ we'll need a few tricks based on the vector model and the following relationships for the Clebsch Gordan coefficients

$$C_{j_1,m_1,j_2,m_2}^{j_3,m_3} = (-1)^{j_2+m_2}\sqrt{\frac{2j_3+1}{2j_1+1}}C_{j_2,-m_2,j_3,m_3}^{j_1,m_1} = (-1)^{j_1-m_1}\sqrt{\frac{2j_3+1}{2j_2+1}}C_{j_3,m_3,j_1,-m_1}^{j_2,m_2},$$
(6.10)

which means that

$$\sum_{\Lambda,m_1,m_2}\left|C_{12}^{L\Lambda}\right|^2 m_1^p$$

$$= \frac{2L+1}{2j+1}\sum_{\Lambda,m_1,m_2}\left|C_{j,m_2,L,\Lambda}^{j,m_1}\right|^2 m_1^p$$

$$= \sum_{m_1}\frac{2L+1}{2j+1}\langle j,m_1|m_1^p(\sum_{m_2}|j,-m_2\rangle\langle j,-m_2|)|j,m_1\rangle$$

$$= \sum_{m_1}\frac{2L+1}{2j+1}m_1^p$$
(6.11)

For more complicated sums we need the vector model in which, for the coupling of two momenta $\mathbf{j_1}+\mathbf{j_2}=\mathbf{L}$, we have

$$\langle L\Lambda|j_{1i}j_{2k}|L\Lambda\rangle = \langle aL_iL_k+b\delta_{ik}+ic\varepsilon_{ijk}L_k\rangle,$$
(6.12)

where a, b and c are coefficients to be found. Evaluating the expectation value of ${\bf j_1}^2$ and $({\bf j_1} \cdot {\bf L})^2$ in the state $|L\Lambda\rangle$ we get

$$
{\bf j_1}^2 = a{\bf L}^2 + 3b, \quad ({\bf j_1} \cdot {\bf L})^2 = \left(\frac{{\bf L}^2 + {\bf j}_1^2 - {\bf j}_2^2}{2} \right)^2 = a{\bf L}^4 + (b+c){\bf L}^2, \tag{6.13}
$$

where ${\bf L}^2 = L(L+1)$, and ${\bf j}^2 = j(j+1)$. Coefficient c can be found by evaluating commutator $[j_i, j_j]$ and using a usual vector model for $\langle L\Lambda | j_i | L\Lambda \rangle$, which gives

$$
c = \frac{1}{4} - \frac{a}{2}. \tag{6.14}
$$

In our case ${\bf j_1}^2 = {\bf j_2}^2 = {\bf j}^2$ and from Eqs. (6.13)

$$
a = \frac{3{\bf L}^2 - 4{\bf j}^2 - 3}{8{\bf L}^2 - 6},
$$

$$
b = \frac{4{\bf L}^2{\bf j}^2 - 2{\bf j}^2 - {\bf L}^4 + {\bf L}^2}{8{\bf L}^2 - 6},
$$

$$
c = \frac{{\bf L}^2 + 3{\bf j}^2}{16{\bf L}^2 - 12}, \tag{6.15}
$$

where ${\bf L}^4 = L^2(L+1)^2$.

It is convenient to collect the following elements together:

$$\langle m^2 \rangle = \frac{1}{2j+1} \sum_{m=-j}^{j} m^2 = \frac{1}{3}j(j+1),$$

$$\langle m^4 \rangle = \frac{1}{15}j(j+1)(3j^2+3j-1) = \frac{1}{5}\langle m^2 \rangle (9\langle m^2 \rangle - 1),$$

$$\sum_{\Lambda,1,2} \left| C_{1,2}^{L,\Lambda} \right|^2 m_1^2 = \frac{1}{3}(2L+1)j(j+1),$$

$$\sum_{\Lambda,1,2} \left| C_{1,2}^{L,\Lambda} \right|^2 m_1 m_2 = \sum_{\Lambda,1,2} \left| C_{1,2}^{L,\Lambda} \right|^2 (\frac{1}{2}\Lambda^2 - m_1^2) = \frac{1}{6}L(L+1)(2L+1) - \frac{1}{3}(2L+1)j(j+1),$$

$$\sum_{\Lambda,1,2} \left| C_{1,2}^{L,\Lambda} \right|^2 m_1^4 = \frac{1}{15}(2L+1)j(j+1)(3j^2+3j-1),$$

$$\sum_{1,2} \left| C_{1,2}^{L,\Lambda} \right|^2 m_1^2 \Lambda^2 = a\Lambda^4 + b\Lambda^2,$$

$$\sum_{\Lambda,1,2} \left| C_{1,2}^{L,\Lambda} \right|^2 m_1^2 m_2^2 = \frac{1}{15}(2L+1)j(j+1)(3j^2+3j-1) + \sum_{\Lambda}(\frac{1}{2}-2a)\Lambda^4 - 2b\Lambda^2,$$

$$\sum_{\Lambda,1,2} \left| C_{1,2}^{L,\Lambda} \right|^2 (m_1^3 m_2 + m_1 m_2^3) = -\frac{2}{15}(2L+1)j(j+1)(3j^2+3j-1)$$

$$+ \sum_{\Lambda}(3a - \frac{1}{2})\Lambda^4 + 3b\Lambda^2, \tag{6.16}$$

Some of these identities follow directly from $\Lambda^2 = (m_1 + m_2)^2$.

6.3 An expression for $\langle H^2 \rangle$

For the sake of completion the result of the statistical theory for the equilibrium value of $\langle H^2 \rangle$ is stated here without derivation.

$\langle H^2 \rangle$ is given by the statistical theory as:

$$\langle H^2 \rangle = \sum_{L,L'} V_L V_{L'} \left(\frac{N}{\omega}\right)^4 [(2L+1)(2L'+1)(1-\frac{4}{2j+1}) + (2L+1)\delta_{LL'}$$

$$+ \frac{9\mathbf{J}^2}{N^2\mathbf{j}^4}((\frac{1}{6}\mathbf{L}^2 + \frac{1}{6}\mathbf{L}'^2 - \frac{2}{3}\mathbf{j}^2)(1 - 8\frac{(2L+1)(2L'+1)}{2j+1} - (2L+1)\delta_{LL'})$$

$$- \frac{4}{3}\mathbf{j}^2 + 4(2L+1)(2L'+1)\sum_L (2L+1)\left\{\begin{array}{ccc} j & j & L \\ L' & j & L \end{array}\right\}(\frac{1}{6}\mathbf{L}^2 - \frac{1}{3}\mathbf{j}^2)$$

$$- 4(2L+1)^2\delta_{LL'}\sum_L (2L+1)\left\{\begin{array}{ccc} j & j & L \\ j & j & L \end{array}\right\}(\frac{1}{6}\mathbf{L}^2 - \frac{1}{3}\mathbf{j}^2))] \qquad (6.17)$$

Bibliography

Bibliography

[1] S. Pratt A. Volya and V. Zelevinsky. *Nucl. Phys. A*, 671:617, 2000.

[2] A.A. Anselm. *Phys. Lett. B*, 217:169, 1989.

[3] S.T. Belyaev. *JETP*, 12, 1961.

[4] S.T. Belyaev and V.G. Zelevinsky. *Nucl. Phys.*, 39, 1962.

[5] H. A. Bethe. *Rev. Mod. Phys.*, 9:69, 1937.

[6] R Bijker and A. Frank. *Phys. Rev. Lett.*, 84, 2000.

[7] Aage Bohr and Ben R. Mottelson. *Nuclear Structure*. World Scientific Pub Co, 1968.

[8] N. Bohr. *Nature*, 137:344, 1936.

[9] A. G. W. Cameron. *Can. J. Phys.*, 36, 1958.

[10] G. Casati and Chirikov. *Quantum Chaos: Between order and disorder*. Cambridge University Press, 1995.

[11] G.F. Bertsch C.W. Johnson and D.J. Dean. *Phys. Rev. Lett.*, 80:2749, 1998.

[12] G.F. Bertsch D.J. Dean C.W. Johnson and I. Talmi. *Phys. Rev. C*, 61:014311, 2000.

[13] N. V. Zamfir D. Kusnezov and R. F. Casten. *Phys. Rev. Lett.*, 8(7), 2000.

[14] A. Volya D. Mulhall and V. Zelevinsky. *Phys. Rev. Lett.*, 85, 2000.

[15] F. J. Dyson and M. L. Mehta. *J. Math. Phys*, 4:701, 1963.

[16] J.P. Elliott. *Proc. Roy. Soc.*, 1958.

[17] V. V. Flambaum and F. Izrailev. 56:5144, 1997.

[18] V.V. Flambaum. *Phys. Scr.*, 46:198, 1993.

[19] V.V. Flambaum and G.F. Gribakin. *Prog. Part. Nucl. Phys.*, 35:423, 1995.

[20] V.V. Flambaum and O.P. Sushkov. *Nucl. Phys. A*, 412:13, 1984.

[21] John D. Garrison. *Ann. Phys.*, 30, 1964.

[22] James Gleick. *Chaos: Making a New Science*. Penguin USA, 1988.

[23] W. Greiner and J. A. Marhun. *Nuclear Models*. Springer Verlag, 1996.

[24] I. I. Gurevich. *JETP*, 9:1283, 1939.

[25] F. Iachello and A. Arima. *The Interacting Boson Model*. Cambridge University Press, 1988.

[26] F. Izrailev. *Phys. Rep.*, 196:299, 1990.

[27] N. Huxel P. von Neumann-Cosel C. Rangacharyulu A. Richter J. Enders, T. Guhr. *Phys. Lett. B*, 486:273–278, 2000.

[28] Dimitri Kusnezov L. F. Santos and Ph. Jacquod. *Phys. Lett. B*, 537, 2002.

[29] Edward N. Lorenz. *The Essence of Chaos (The Jessie and John Danz Lecture Series)*. University of Washington Press, 1996.

[30] B.A. Brown M. Horoi and V. Zelevinsky. *Phys. Rev. Lett.*, 87:85, August 2001.

[31] B. Mandelbrot. *Fractal Geometry of Nature*. W H Freeman & Co, 1988.

[32] M. L. Mehta. *Random Matrices*. Academic, New York, 1991.

[33] Alexander Volya Mihai Horoi and Vladimir Zelevinsky. *Phys. Rev. Lett.*, 82:2064, 1999.

[34] and V. Zelevinsky N. Frazier, B.A. Brown. *Phys. Rev. C*, 54:1665, 1996.

[35] T. D. Newton. *Can. J. Phys.*, 34, 1956.

[36] M. J. Giannoni O. Bohigas and C. Schmidt. *Phys. Rev. Lett.*, 52:1, 1984.

[37] Heinz-Otto Peitgen and Peter H. Richter. *Beauty of Fractals: Images of Complex Dynamical Systems*. Springer Verlag, 1988.

[38] A. Pandey R. Haq and O. Bohigas. *Phys. Rev. Lett.*, 48:1986, 1982.

[39] G. Racah. *Phys. Rev.*, 78, 1950.

[40] T. Døssing *et al. Phys. Rev.*, 268, 1996.

[41] Hans-Jurgen Stockmann. *Quantum Chaos: An Introduction*. Cambridge University Press, 1999.

[42] G. Kilgus *et al. Z. Phys. A*, 326:41, 1987.

[43] T.A. Brody *et al. Rev. Mod. Phys.*, 53:385, 1981.

[44] N. Frazier V. Zelevinsky, B.A. Brown and M. Horoi. *Phys. Rep.*, 276:85, 1996.

[45] F. Izrailev W. Wang and G. Casati. 57:323, 1998.

[46] H. Vonach W.Dilig, W. Schantl and M. Uhl. *Nucl. Phys. A*, 217, 1973.

[47] A. Arima Y. M. Zhao and N. Yoshinaga. *nucl-th/0206040*.